9601

# The Photoproduction of Neutral Pions in Hydrogen.

by

D.B. Miller.

Presented to the University of Glasgow as a thesis for the degree of Doctor of Philosophy, January 1962.



ProQuest LLC.
789 East Eisenhower Parkway
P.O. Box 1346
Ann Arbor, MI 48106 – 1346

# Preface.

The following thesis describes the research performed by the author in the Department of Natural Philosophy of the University of Glasgow from October 1956 to September 1961, in conditature for the degree of Doctor of Philosophy.

Chapter I is a summary of the relevant theoretical attempts to describe the photoproduction of mesons in hydrogen.

Chapter II is a review of experimental methods and knowledge in low energy neutral pi-meson photoproduction.

In Chapter III consideration is given to the experimental measurements of those properties of bremsstrahlen beams whose value is essential for the absolute measurement of photoproduction processes. Some previous results in this field are given a new interpretation.

Chapter IV describes a new and improved form of liquid hydrogen target designed and developed by the author for this work. This has proved of wide application in photomeson work.

Chapter Vcontains a description af a counter telescope and electronic measurement apparatus with some novel features which were designed and built by the author.

Chapter VI describes the performance of the experiment and analysis of the data. The collection of data was possible only with the generous help of Dr. W.R.Hogg and Mr.H.C.Evans. The analysis and interpretation of the results (Chapter VII) was the work solely of the author.

Work of this nature is built on a foundation of experience gathered by all members of the laboratory, and the author is grateful to all of them for their ready advice and assistance.

I am indebted especially to my supervisor Professor E.H. Bellamy for much helpful discussion and advice during the first three and a half years of this work.

The author owes his introduction to low temperature techniques primarily to Dr. W.R. Hogg and is grateful to him for many useful discussions and suggestions on this and other subjects during the work.

The assistance and advice of Dr. P.Palit was invaluable during the early stages of the development of the electronics.

The investigations leading to the present reliable state of the synchrotron X ray monitor ion current integrator were shared with Mr. H.C.Evans.

The effort to achieve consistency in the absolute energy flux calibration of the synchrotron beam has been the work of Mr. T. Aitken, Dr. W. McFarlane, Mr. E. Gabathuler, Mr. E. Lawson and the author.

Much is owed to the technical and workshop staff for their assistance.

In conclusion I would to thank Professor P.I. Dee for his keen interest in this work and Dr. McFarlane and his assistants for patiently providing many hours of synchrotron beam.

I am also grateful to the Department of Scientific and Industrial Research and the Court of the University of Glasgow for financial support.

## Publications.

1. A thin liquid hydrogen or deuterium target.

   E.H.Bellamy, W.R.Hogg and D.Miller

   Nuclear Instruments and Methods 7, 293 (1960).

2. $\pi^+$ photoproduction from hydrogen near threshold.

   J.G.Rutherglen, J.Walker, D.Miller and J.M.Patterson.

   Proceedings of the 1960 Annual International Conference on high energy physics at Rochester p.23.

3. A level controller for liquid nitrogen.

   D.Miller and H.C.Evans.

   Journal of Scientific Instruments 38, 162 (1960).

4. The spectator model in photomeson production in deuterium.

   H.C.Evans, D.Miller and E.H.Bellamy

   To be published.

## Publications (contd.)

5. $\pi^{o}$ photoproduction in hydrogen at $90^{o}$ in centre of mass system.

D. Miller and E.H. Bellamy.

To be published.

# Index.

## Chapter I.

### Theoretical Introduction.

In 1935 Yukawa introduced the concept of mesons, analagous to the photons of the electromagnetic field, in an attempt to explain the strength of nucleon-nucleon forces. When, with the advent of high energy accelerators, it became possible to produce these particles artificially, the collisions of mesons with nucleons and nuclei were studied to obtain information relating to nuclear properties. This led eventually to the discovery of a whole spectrum of particles with strong interactions with nucleons, and the study of these and other elementary particles now constitutes a major branch of physics.

The basic properties of free $\pi$ - mesons (mass, spin etc.) were early measured (see for example Bethe and de Hoffmann (1955)) and subsequently activity has concentrated on investigations of the details of their interactions with nucleons. This can be done most obviously by the scattering of mesons by nucleons, more indirectly by the photoproduction of mesons at nucleons (which involves also the electro-magnetic field, but this is thought to be well known) and the production of mesons in nucleon-nucleon collisions.

The most obvious features of the early results of photoproduction of pions at nucleons were

1. The pronounced peaking in the total cross-section at photon energies about 300 Mev (corresponding to a similar peak in the $\pi$ - nucleon scattering results at 190 Mev)
2. The orders of magnitude of charged and neutral meson photoproduction cross-sections were about the same.
3. The dependence on photon energy $E\gamma$ of the cross-sections just above threshold was

   $(E\gamma - Eo)^{3/2}$ for $\pi^o$ mesons and

   $(E\gamma - Eo)^{1/2}$ for $\pi^+$ mesons from hydrogen,

   where Eo is the photon energy at the threshold from meson production.

Early attempts to explain these results theoretically (the so-called weak and strong coupling theories) led to conflict with experiment.

More success was obtained by the phenomenological theories, such as that of Feld (1953). This does not assume a specific model for the $\pi$ - meson production. Using very general arguments about the conservation of angular momentum and parity during the process, it derives the angular distribution to be expected from the

transition from initial to final states of known angular momentum and parity, and the momentum dependence of the cross-section to be expected near threshold.

The known strong peaking at $90^{o}$ in the centre of mass system and the $(E\gamma - Eo)^{\frac{3}{2}}$ dependence of the total cross-section near threshold suggests that the photoproduction of $\pi^{o}$ mesons proceeds almost entirely through a meson - nucleon state with spin and isotopic spin $\frac{3}{2}$ . This predominance of the $(\frac{3}{2}, \frac{3}{2})$ state is in agreement with the pion scattering evidence. However the interference between different states can give rise to a term containing $\cos\theta$ , and it has been conventional to fit the angular dependence in the centre of mass system by an expression

$$\frac{d\sigma}{d\Omega} = A + B\cos\theta + C\cos^{2}\theta \qquad (1)$$

($\theta$ is angle of pion production in c.m. system)

with A,B and C functions of $\gamma$ ray energy. For $\pi^{o}$ production A and C are large (C is negative) and B is small. With this expression, good fits have been made to the experimental data up to $E\gamma$ = 450 Mev. (see chapter II, figure 1), but the relation between A and C given by simple considerations, C/A = -0.6

was found to be invalid below $E_\gamma$ = 200 Mev. (Koester and Mills (1957)).

A relatively successful attempt to interpret the increasing amount of experimental data was made by Chew and Low (1956). Returning to the basic Yukawa theory, some of the difficulties in the straight forward approach were removed by enlarging the region of the pion-nucleon interaction to a finite size, instead of a point. This size introduced an additional parameter into the theory, and comparatively good fits were obtained to experiment, particularly in the resonance region

The application of relativistic dispersion theory to the problem of pion photoproduction was made by Chew, Goldberger, Low and Nambu (1957). This theory and its developments give the best basis for the prediction of results in photomeson production. In this theory too, the results for $\pi^o$ photoproduction can be expressed in the form (1) and expressions for A,B and C have been calculated by Hohler and Mullensiefen (1959) and Dietz, Hohler and Mullensiefen (1960) from the phase shifts derived from $\pi^-$-nucleon scattering.

Detailed consideration of the results of those calculations are deferred to chapter VII.

This thesis describes measurements made of the value of A, the angular independent part of the cross-section for $\pi^o$ photo-production in hydrogen. These measurements differ considerably from previously accepted values in some regions.

## Chapter II.

Review of published work.

1. Methods of measurement.

The photon sources available for the photoproduction of mesons all have continuous spectra formed by the nuclear collision of fast electrons. However in reactions which involve only two real particles at any one time, observation of the angle and energy of any one particle, or corresponding parameters, can yield both the photon energy and differential cross-sections.

Thus four methods are generally used for measuring the photoproduction of neutral $\pi$ mesons at protons

$$\gamma + p \longrightarrow \pi^0 + p \qquad (2)$$

A. Measurement of the energy and angle with respect to the photon beam of the recoil proton. The difficulty of detecting low energy protons at certain angles limits the range of this method. Also the protons have a high $dE/dx$ and if the detector is placed outside the target, the target must be thin, with consequent low counting rate. If the target ( e.g. polythene) contains complex nuclei then the photodisintegration of these swamps the protons produced by (2 ). This can be overcome by

B. measuring the proton in time coincidence with at least one of the photons from the $\pi^o$ decay. In general the photon counter will not be 100% efficient which introduces some uncertainty. The small proton content of compound targets of thickness small enough for measurement of low energy proton recoils is also disadvantageous.

C. Alternatively measurements can be made on the $\pi^o$ meson. This decays rapidly ( $\lesssim 10^{-16}$sec.) into two high energy photons. The angles and energies of these photons are directly related to the angle and energy of the original $\pi^o$, but the poor energy resolution of available high energy photon counters produces much smoothing of the cross-sections resulting from such experiments.

D. Experiments have also been done by counting only one of the $\pi^o$ decay photons. The direction of the $\gamma$-ray bears a statistical relationship to the direction of the $\pi^o$ meson ( as has been elaborated by Koester and Mills (1957) and Vasilkov et al.(1959)). This is used, together with a means (such as the photon difference method) of identifying the energy of the photon responsible for the reaction. This method also results in much averaging over angle and energy.

2. Results.

The first observations of the photoproduction of $\pi^o$ mesons were made by Steinberger et al (1950) and Panofsky et al. (1952) at Berkley using method C. They showed that the cross-section for reaction (2 ) rose slowly from threshold to 300 Mev, with a magnitude about that of charged meson production.

The first accurate measurements on production at protons were reported by Silverman and Stearns (1952) using method B and Cocconi and Silverman (1952) with method D. More detailed results followed from Goldschmidt-Clermont et al. (1955), Oakley and Walker (1955) both using method A and by Walker et al. (1955) using B.

These later results (the absolute values of results prior to 1955 are subject to some 30% uncertainty) represent all the published results available at the beginning of the work described in this thesis.

Since 1956 the lower energy region has been investigated by Koester and Mills (1957) with methods D and A. They showed that, below $E_\gamma$ = 200 Mev, their results were inconsistent with C/A = -0.6 and B = 0.

McDonald et al. (1957) with method A obtained results up to $E_\gamma$ = 450 Mev. He combined these results with those

of Oakley and Walker and Goldschmidt-Clermont et al. at 260 Mev and with Oakley and Walker at 300 Mev to obtain the results shown against McDonald et al. in figure 1 .

Smythe et al.(1957) repeated and extended these measurements.

De Wire et al.(1958) made measurements with method B from 300 to 1000 Mev.

A series of measurements at high ( > 500 Mev) energies were made by Stein and Rogers (1958) Vette (1958) and from 250 to 1000 Mev by Berkelman and Waggoner (1960). The last named combined these results with those of McDonald et al. and Oakley and Walker to give the results shown under Berkelman and Waggoner in figure 1 .

Measurements at low energies, by method D have been made by Luckey et al. (1959) and by Vasilkov et al. (1959).

The results shown in figure 1 are most of the published data. The absolute values of some results (Walker et al., Oakley and Walker, McDonald et al., Smythe et al., and Berkelman and Waggoner) have been increased by 4.5%. This is to bring the calibration constant assumed for the photon flux measuring ionisation chamber into line with that adopted here.(See chapter 3.)

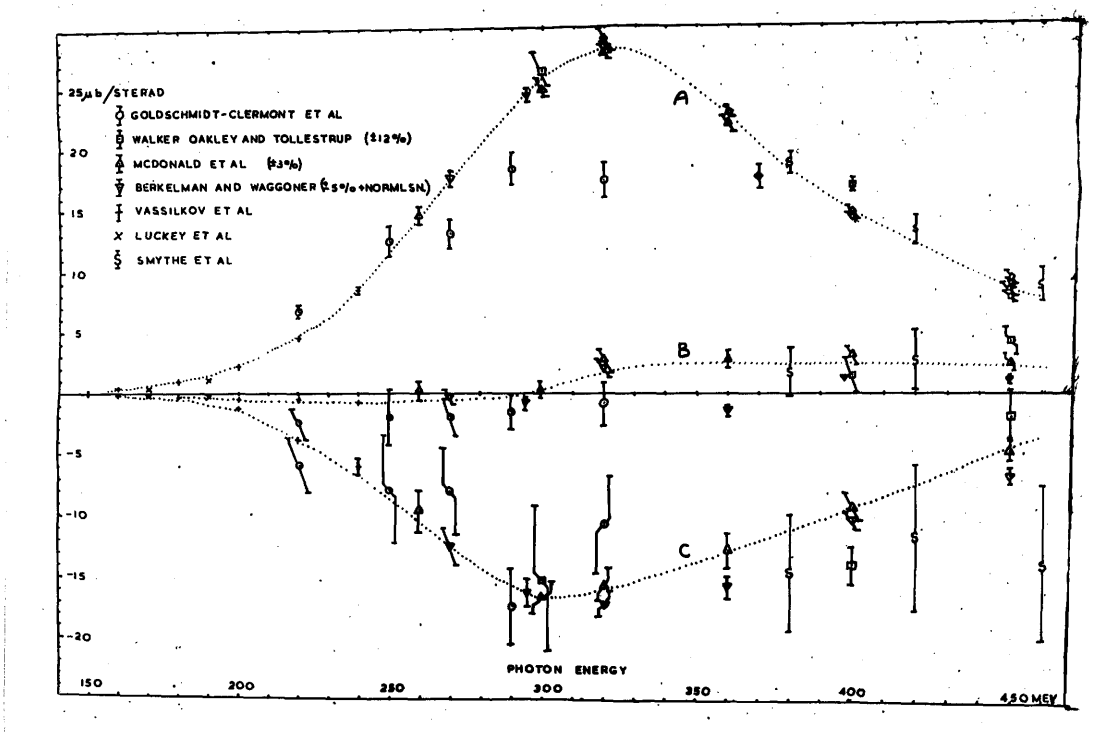
25 μb/STERAD
GOLDSCHMIDT-CLERMONT ET AL
WALKER OAKLEY AND TOLLESTRUP (±12%)
MCDONALD ET AL (±3%)
BERKELMAN AND WAGGONER (±5%+NORMLSN)
VASSILKOV ET AL
LUCKEY ET AL
SMYTHE ET AL
A
B
C
20
15
10
5
-5
-10
-15
-20
150
200
250
300
350
400
450 MEV
PHOTON ENERGY

fig. 1

The absolute value of the results of Vasilkov depends on the $C^{12}$ ($\gamma$, n) $C^{11}$ activation reaction cross-section .

Some other spot measurements ( e.g.Bernardini et al. (1960)) made at different angles and energies have not been included in the above analysis. (See chapter VII).

It should be noted that the 260 Mev points of McDonald et al. depend strongly on the measurements of Oakley and Walker and Goldschmidt-Clermont et al. The 300 Mev points depend strongly on measurements by Oakley and Walker. The results of Berkelman and Waggoner were uncertain by a factor due to the boiling of their relatively unshielded liquid hydrogen target. They nominalised them to those of McDonald et al. at a common point at 340 Mev.

The absolute values of the independent results shown have further uncertainties ( due, for example, to the different ways of finding the photon intensities, or the efficiency of counters). The experimenters own estimates of these are noted on figure 1 .

Because of the mutual dependence and disagreement of the results shown in figure 1 it was deemed worthwhile to obtain independent results over as wide a range of photon energies as possible. The rest of this thesis describes the method used and the results obtained for the value of the coefficient A for photons between

200 and 300 Mev. The most accurate method available for this range is measurement of the recoil proton spectra.

## Chapter III.

The photon beam.

### 1. Introduction.

Since much of the uncertainty in the final cross-sections and many of the experimental parameters were set by the available high energy photons, these are considered first.

The measurements were made using the bremsstrahlung beam of the Glasgow University 320 Mev electron synchrotron. The operation of this machine has been described by McFarlane et al.(1955) and Atkinson et al. (1957), but a brief resume of the most important details relative to the mode of operation during this experiment is given.

Electrons were accelerated by a radiofrequency electric field up to 320 Mev in a circular orbit in a pulsed( 5 times/ second) magnetic field. About 1 millisecond before the peak magnetic field occurred, the amplitude of the r.f. voltage was slowly reduced causing electrons which had a large amplitude of phase oscillation to lose synchronism. Losing energy by radiation at the rate of about 800 ev. per revolution, they slowly spiralled-in in the almost constant magnetic field until they struck a target consisting of a 0.15 cm. diameter tungsten wire normal to the plane of the orbit. Collisions in the outmost edge of the wire caused a tangential cone-shaped beam of bremsstrahlung as shown in figure 2.

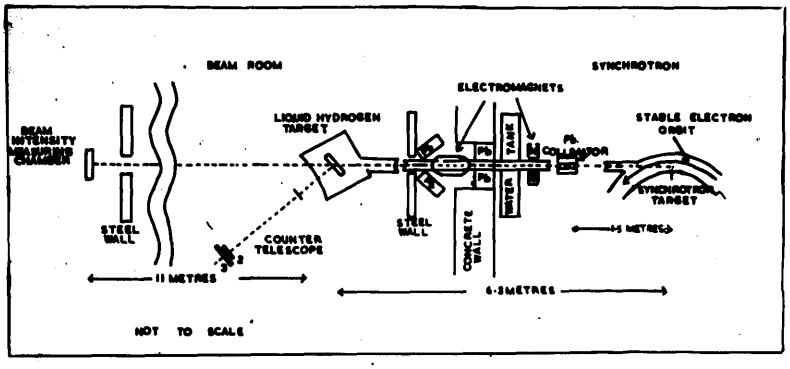
BEAM ROOM
SYNCHROTRON
ELECTROMAGNETS
LIQUID HYDROGEN TARGET
STABLE ELECTRON ORBIT
BEAM INTENSITY MEASURING CHAMBER
Pb
TANK
Pb COLLIMATOR
SYNCHROTRON TARGET
STEEL WALL
COUNTER TELESCOPE
STEEL WALL
CONCRETE WALL
WATER
11 METRES
6·3 METRES
NOT TO SCALE

fig. 2

By suitable modulation of the r.f. amplitude the bremsstrahlung beam pulse was spread out over a period of about 2 ms., 1 ms. either side of peak field. This reduced the instantaneous counting rates in the experimental particle detection system to operable values.

The electron energy corresponding to a circular orbit at the target radius at the peak field was calculated (via a calibration due to McFarlane) from the voltage of the condenser bank which was discharged to pulse the magnet. This gave 318 $\pm$ 2 Mev at the peak value of the magnetic field pulse, and hence 309 Mev at the instants 1 millisecond before and after peak field, with a corresponding energy modulation in the bremsstrahlen.

2. X-ray beam path. (figure 2).

After leaving the do-nut through a thin window, the axial portion of the X-ray cone was selected by passing it through a 1/4" hole in a 9" long, 4.1/2" diameter lead cylinder 125 cm. from the tungsten target. The selected centre portion then entered an evacuated pipe which passed through the gap of an electromagnet to deflect charged particles out of the beam, then through a shielding wall of water, barytes concrete and lead to the experimental area. Here the beam passed through only 1.1/2" of air on its way into the liquid hydrogen experimental target. The distance from the synchrotron target to the liquid hydrogen target was 6.3 metres, and at this point the cross-section of the beam

was elliptical about 4.0 cm. vertically and 3.0 cm.horizontal After passing through the experimental target, the beam continued through 11 metres of air to the far end of the beam room where its intensity was measured in an ionisation chamber with thick copper walls (see § 4).

The position of the beam for accurate lining up of apparatus was found by exposing photographic films in it behind suitable converters, as described in chapter 4.

## 3. Energy spectrum of beam.

The bremsstrahlung spectrum of electrons in the nuclear field was calculated by Bethe and Heitler (1934). The contribution by bremsstrahlung in the field of the atomic electrons was calculated by Wheeler and Lamb (1939). Various experimental checks have been made of this theory (e.g. Curtis (1953), Fisher (1953),Haggerman and Crowe (1955) Bernstein and Panofsky (1956)) and of the related pair production cross-section. These found that with high Z targets and energies $>$ 20 Mev the Bethe-Heitler theoretical predictions were $\sim$ 10% too high. Better agreement was found using different approximations by Bethe and Maximon (1954) and Olsen et al. (1957).

The application of theory to this case is complicated by several considerations. The rate of spiralling-in of the electrons to the target is $\sim 10^{-3}$ cm. radially per revolution. The target is a 0.15 cm. diameter wire

so the first traversal of the target is at the thinner outer edge at an average thickness of 0.01 cm. The ionisation energy loss in 0.01 cm. of tungsten is $\sim$ 0.5 Mev and is sufficient to seriously disturb the electron orbit so that it probably misses the target on subsequent revolutions. Thus the effective target thickness is much less than the diameter of the wire. The r.m.s. angle of multiple scattering of 320 Mev electrons in 0.01 cm of tungsten is $\sim 1.2 \times 10^{-2}$ radians, the angular spread characteristic of bremsstrahlung is $^{mec^2}/E \sim 1.5 \times 10^{-3}$ radians. So the angular spread of the bremsstrahlen is about 4 times that due to the bremsstrahlung process itself. This results in a photon intensity distribution with energy different from that given by the forward production on the above theories. Several calculations of these effects (Schiff (1946, 1951), Hisdal (1957) Sirlin (1957) ) have been made, but are not directly applicable because of the uncertainties in the details of the process outlined above. Only the central part of the beam is selected by the collimator, up to $\pm 2 \times 10^{-3}$ radians.

Measurements ( e.g. Powel et al. (1951) De Wire and Beach (1951), Diambrini et al. (1961)) have been made of the photon spectrum emerging from such a collimation system, using pair spectrometers. At 300 Mev De Wire and Beach

found agreement within 3% with the Bethe-Heitler predictions when a thin ($1.25 \times 10^{-3}$cm) tungsten target was used in the synchrotron. With a 0.10 cm. target, the ratio of the numbers of 250 and 50 Mev photons was 5 to 10% lower than predicted. More accurate (1%) measurements at 1 Gev by Diambrini et al. showed a similar effect. For a thin target (0.013 radiation lengths) the depression below the Bethe-Heitler predictions at the high energy end of the spectrum depended on the width of the collimator, being zero for a narrow one. For a thick target (0.13 radiation lengths) the depression was about 10% for photons of 95% of the maximum energy for both wide and narrow collimators.

Figure 3 shows the measurements of J.K.Walker and J.G.Rutherglen (Walker 1961) made on the Glasgow synchrotron with the target and collimation system used in the present experiment. Evidently a depression of 10% ($\pm$ 4%) at $E/Eo$ = 0.95 in agreement with other measurements also fits their results better than the Bethe-Heitler spectrum. The dotted line shows this spectrum corrected for the further depression caused by the spreading out in time to a greater extent in this experiment than during the spectrum measurements. All these corrections to the theoretical formula are negligible below $E/Eo$ = 0.75.

The difference in area between the Bethe-Heitler curve and the experimental line is only 0.8 $\pm$ 0.2%. Further corrections to the total energy (area) may be necessary

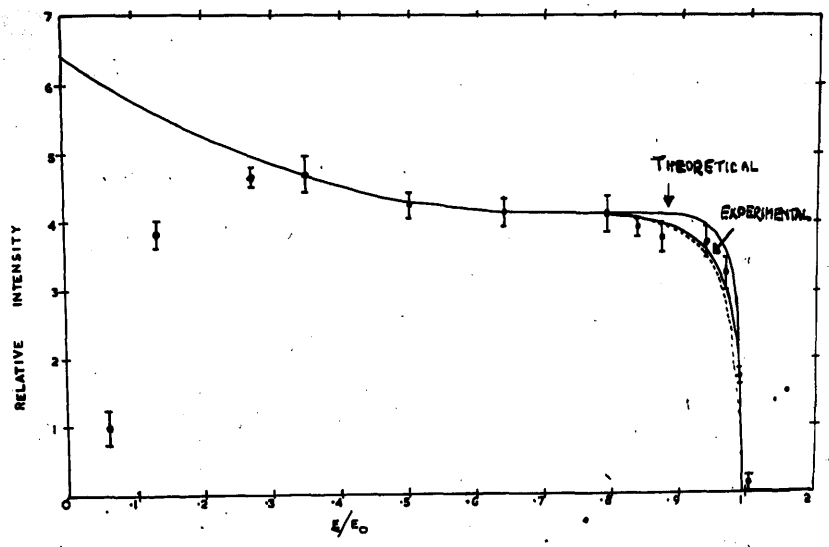


fig. 3

due to the deviations from the theoretical expressions at energies $< 0.3\ E_{max}$, where pair spectrometer measurements become difficult. It is unlikely that these will amount to more than 1% (Diambrini).

4. The absolute intensity of the photon beam.

It is usual to characterise the intensity of high energy bremsstrahlung beams in terms of the total flux of energy in the beam.

Thus

Number of equivalent quanta/minute = Q/min

$$= \frac{\text{integrated energy flux/minute}}{\text{peak energy of beam.}}$$

When the spectral distribution and Q are known, the flux of photons within any energy interval can be calculated. The intensity of the synchrotron beam during this experiment was about $10^9$ equivalent quanta/minute.

This was measured in a "Cornell thickwalled ionisation chamber" (Corson et al.(1953)) with plane parallel 1" thick copper walls seperated by 1" with a 1/16" thick copper collecting electrode halfway between. The gap is open to the atmospheric air. The beam enters normally through one wall and in the copper an electron - photon shower develops, which has its maximum density of ionisation in the air gap. The ion current is proportional to the Q of a photon beam of fixed energy. After use, the chamber was dismantled and it was found that its important dimensions were all correct to $\lesssim$ 0.5%.

A number of absolute calibrations (in terms of coulombs of charge collected per MeV of energy in beam) have been reported for this chamber at different energies. Since the number and accuracy at 310 MeV is small, a range of peak bremsstrahlen energies has been included in figure 4, and an empirical best fit (straight line) drawn through them.

Loeffler et al. (1959) give a different calibration and energy dependence. Figure 5. These were based on absolute measurements included in figure 4, and relative measurements made with a pair spectrometer and activation method sensitive only to photon below 75 and 40 MeV respectively. Their choice of standardisation points gives agreement at 310 MeV, but on extrapolation they give a different factor for the normalisation of early experiments at California Institute of Technology (Chapter II). The discrepancy may be due to the energy sensitivity of their methods being limited to the part of the spectrum to which the ionisation chamber is least sensitive.

Another ionisation chamber for the measurement of high energy bremsstrahlen has been described by Wilson (1957). This "Quantameter" has an energy independent calibration which can be calculated theoretically to an

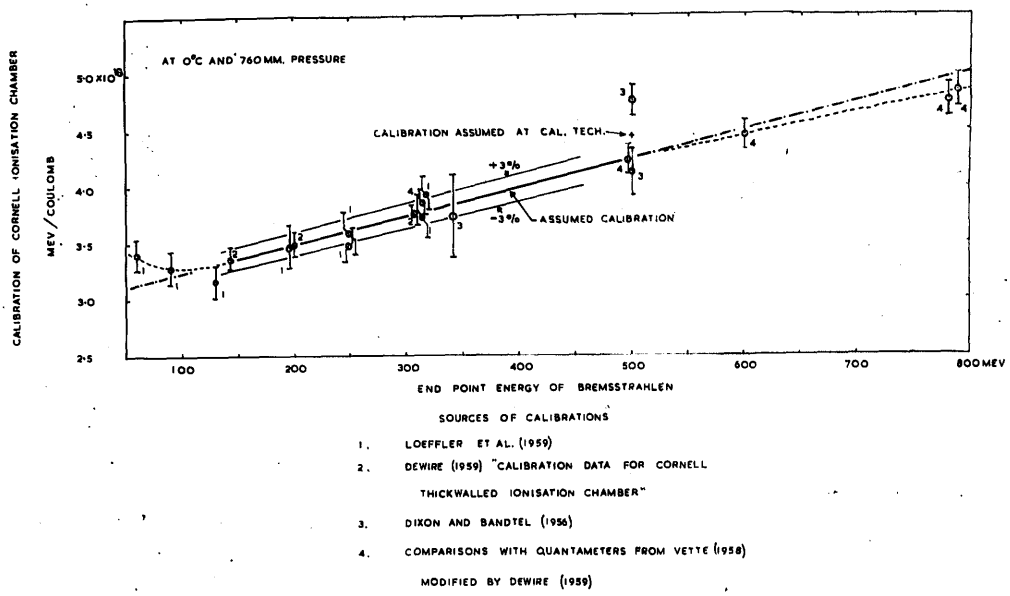
CALIBRATION OF CORNELL IONISATION CHAMBER
MEV/COULOMB
AT 0°C AND 760 MM. PRESSURE
CALIBRATION ASSUMED AT CAL. TECH.
+3%
-3%
ASSUMED CALIBRATION
END POINT ENERGY OF BREMSSTRAHLEN
SOURCES OF CALIBRATIONS
1. LOEFFLER ET AL. (1959)
2. DEWIRE (1959) "CALIBRATION DATA FOR CORNELL THICKWALLED IONISATION CHAMBER"
3. DIXON AND BANDTEL (1956)
4. COMPARISONS WITH QUANTAMETERS FROM VETTE (1958) MODIFIED BY DEWIRE (1959)

fig. 4

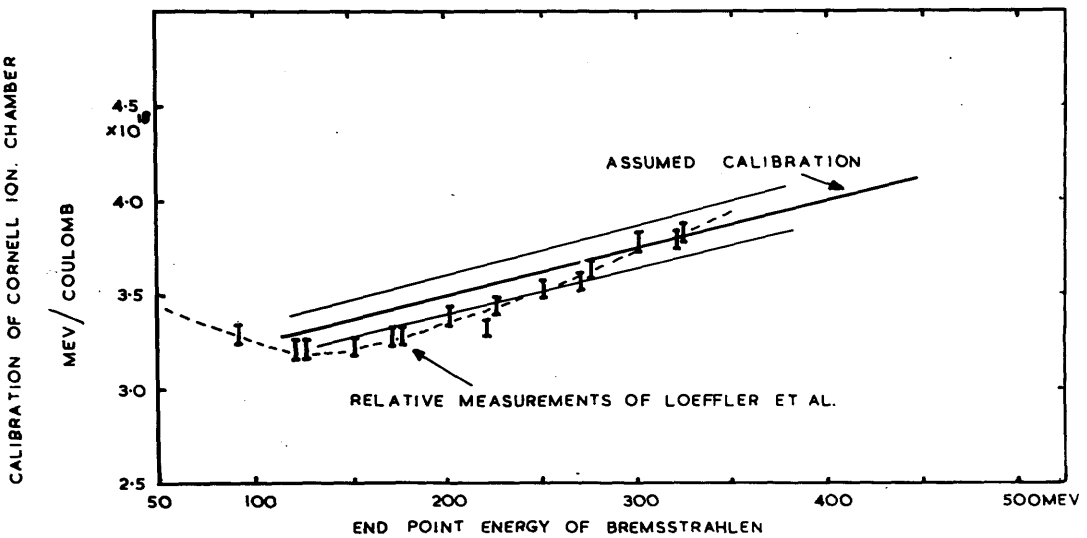
CALIBRATION OF CORNELL ION. CHAMBER
MEV/COULOMB
ASSUMED CALIBRATION
RELATIVE MEASUREMENTS OF LOEFFLER ET AL.
END POINT ENERGY OF BREMSSTRAHLEN

fig. 5

accuracy of ± 3%. Several intercalibrations of this with the Cornell thick-walled chamber are given in figure 4.

The agreement between all these measurements, made under different conditions with different methods lends confidence to the value of the calibration at 318 Mev of $3.78 \times 10^{18}$ ( ± 3%) Mev/coulomb used in this experiment.

The ion current from the chamber was integrated electronically. The linearity and stability of this integrator was repeatedly checked throughout the experiment and ( after a method was found for subtracting a residual drift in the zero point of the integrator) the r.m.s. deviation from the mean calibration during the experiment was ± 0.7% at the level of the average beam intensity. An absolute calibration accurate to ± 0.5% was made by discharging into its input an accurately known capacity charged to a known voltage. A recalibration some seven months later gave the same value within 1%.

The uncertainty in the relative number of photons in different runs is ± 1% ( from integrator stability and linearity) for photons between 200 and 240 Mev. This rises to ± 3.5% at 300 Mev, owing to the additional uncertainty in the spectrum.

The uncertainty in the absolute photon numbers includes also ± 3% from the absolute calibration of the Cornell chamber, ± 1.2% from the area under the photon spectrum and ± 0.5% from the absolute calibration of the integrator, i.e. an additional 3.4%.

Thus the uncertainty in absolute numbers of photons is ± 3.5% between 200 and 240 Mev rising to 4.9% at 300 Mev.

A measured correction of (7.0 ± 0.5) % was applied to the calculated absolute number of photons due to absorbers placed immediately in front of the Cornell ionisation chamber.

## Chapter IV

### The target of protons.

1. Specification.

The reaction is to be studied by passing a collimated bremsstrahlung beam through a target of almost stationary protons, and sorting the recoiling protons by energy and angle to the incident beam. This at once restricts the possible forms of the target. Because of the effects of nuclear binding and momentum distribution, the target material is restricted to hydrogen in elementary or chemical compound form. The reaction cross-section and the available photon flux are both small, so to obtain statistically well defined answers in a few weeks running time, the thickness of the target must be of the order of 0.1 gm/cm$^2$. If the detector is to be placed outside the target, a maximum allowable target thickness is specified by the uncertainty in energy of recoil introduced by differences in energy loss in penetrating different thicknesses of the target. For this experiment this leads to an optimum thickness of about 0.07 gm/cm$^2$ of pure hydrogen. Compound targets are disallowed because of the high flux of protons from the photo-disintegration of the other constituents.

In general this hydrogen will be contained by walls of a different material with more complicated nuclei. The cross-section for the photodisintegration of these nuclei yielding protons which could be confused with recoil protons from $\pi^o$ production is large ( X 100 ) compared with meson photoproduction cross-sections, so the walls themselves must be very thin or else must be kept out of the sensitive region of the detector. Also the cross-section for the Compton scattering of photons and electrons and the production of electron pairs rises with increasing atomic number and leads to the same need for thin or distant walls.

To conveniently achieve the necessary accuracy ($\pm 1\frac{1}{2}^o$) of measurement of the recoil proton angle with a detector of reasonable size, the target must be localised to a region of a few centimetres linear dimensions. For a target of the optimum thickness 0.07 gm/cm$^2$, this means that it must be about 1000 times as dense as hydrogen at N.T.P. This can be done by compressing and cooling the gas, or by liquefying it.

Table 1.

| State | Density |
|---|---|
| Hydrogen gas at N.T.P. | .09 gm/litre |
| Hydrogen gas at 77°K, 2000 lb/sq.inch. | 40 gm/litre |
| Liquid hydrogen (20.4°K, 1 atmosphere) | 70 gm/litre |

The engineering problems involved in making either liquid, or cold compressed gas targets are of about the same difficulty. Both forms of target have been used by previous experimenters.

2. Gas targets.

The disadvantages of the high energy loss in the thick exit windows necessary for the high pressure targets ( which prohibit the use of external detectors for low energies) have been overcome by having the particle detectors inside the pressure vessel in the form of nuclear emulsions ( e.g. Goldschmidt-Clermont et al. (1955)). However the particles have still to traverse several centimetres of dense gas between the active regions of the target and the detector and particles produced, in the thick photon beam windows, and long lengths of gas exposed to the beam but not part of the target volume, may affect the measurements. Accurate calculation of solid angle and actual thickness of the target, depending on a measurement of the angular acceptance of the detectors, and the distance from various parts of the extended photon beam to the extended sensitive area of the detectors, is difficult.

## 3. Liquid targets.

Previously used liquid targets have taken the form of right cylinders with axes either along the beam or at right angles to it , ( e.g. Cook (1951) Whalin and Reitz (1955), Nicolai (1955) Littauer (1958), Berkelman and Waggoner (1960)). These were filled with liquid hydrogen and thermally insulated usually by high vacuum. These targets are of non-uniform thickness, and together with the non-uniform flux distribution in the photon beam, a calculation of the equivalent target thickness is uncertain. If a plane parallel sided target is made, because of the reasons given above, the walls must be thin ( about $10^{-3}$ inches) and so bulge to an extent difficult to measure under running conditions. For liquid targets about 1 cm. thick (0.07 gm/cm$^2$) this is a large effect ( 10% - 100%). However it seemed possible to design a novel form of liquid hydrogen target which overcomes these difficulties. The construction and performance of this target is described below.

## 4. The new form of target chamber.

The disadvantages of earlier liquid targets could be removed if it could be arranged that there was no pressure difference across the thin containing walls.

With vacuum insulation, the pressure difference across the walls is due to the vapour pressure of the target material. So to reduce this, all that needs to be done is to reduce the operating temperature by pumping the refrigerant. For liquid targets a limiting point here is the vapour pressure at the ~~critical~~ triple point (about 5.5 cm of mercury at 14°K for hydrogen). Below this point the hydrogen is solid, which makes possible in principle a wall-less dense hydrogen target. But the mechanical difficulties of this form , including the 10% volume change on solidification were deemed to be too severe.

However from preliminary tests it seemed possible to make a target with only a small bulge by this method, just above the critical point, and a prototype was constructed with thin walls of "Melinex" (terylene)film and was tested to measure the low temperature properties of this material. But with dimensions suitable for practical use, the bulge was still too large under running conditions.

The other approach is to increase the pressure of the gas outside the walls to the same as that inside. The difficulty here is that the density of the surrounding gas is quite high( about 2% of that of liquid hydrogen) so that troubles related to these of high pressure gas targets are experienced.

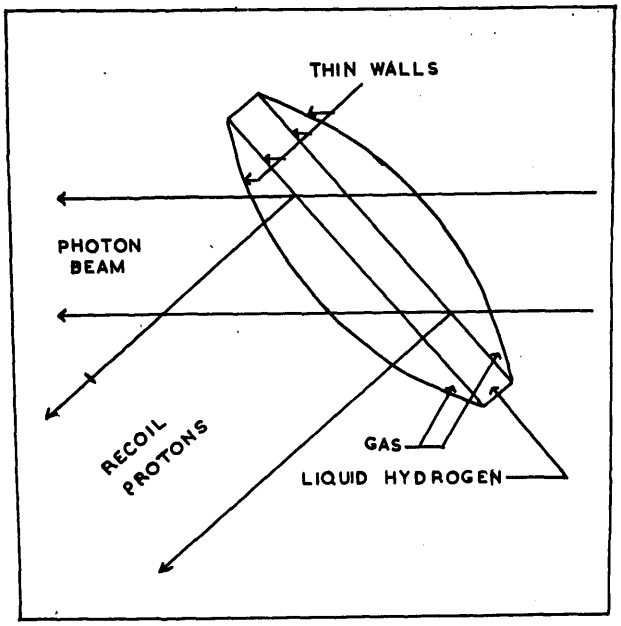
THIN WALLS
PHOTON BEAM
RECOIL PROTONS
GAS
LIQUID HYDROGEN

fig. 7

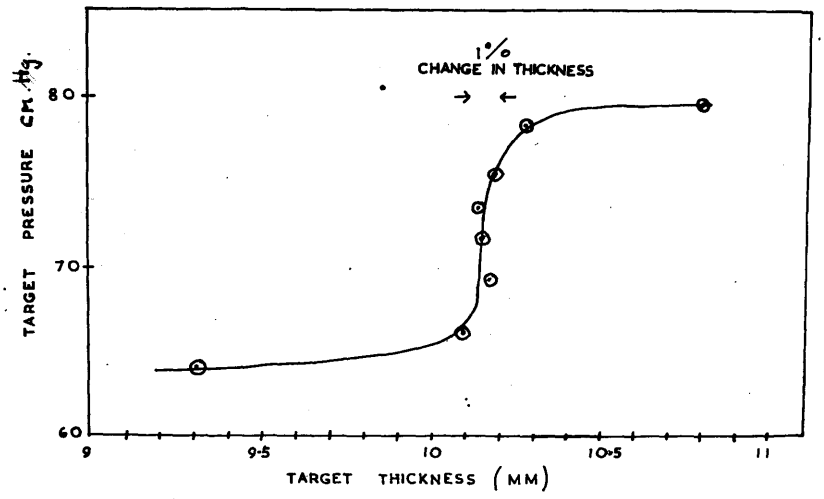
1% CHANGE IN THICKNESS
TARGET PRESSURE CM. Hg.
80
70
60
9
9·5
10
10·5
11
TARGET THICKNESS (MM)

fig. 9

For this experiment the optimum design was a compromise in which a thin layer of gas was kept on either side of a circular disc of liquid hydrogen 1 cm thick, with its axis horizontal. This is illustrated diagrammatically in figure 7. The gas(hydrogen diluted with 1-2% of helium to prevent liquefaction) in the two outer layers was kept at exactly the same pressure as the top layer in the liquid ( which was approximately 1 atmosphere for simplicity.)

The heat received by the target chamber by radiation from the surroundings is dissipated by conduction up to the liquid hydrogen refrigerant boiling at 1 atmosphere pressure as described in § 5. Thus the temperature of the target is higher than the boiling point of liquid hydrogen, so the vapour pressure is greater than 1 atmosphere. To prevent the target liquid from boiling it was made a closed system independent of the hydrogen refrigerant. Changes in its vapour pressure, due to ortho-para conversion in it and in the refrigerant, changes in the barometric pressure and changes in the heat flux, must be transmitted to the two layers surrounding the liquid, because a 1 cm. pressure difference across the walls caused a 25% bulge at the centre. This transmission was achieved by leading pipes out of both the inner and outer chambers to the device shown in figure 8, where they lead

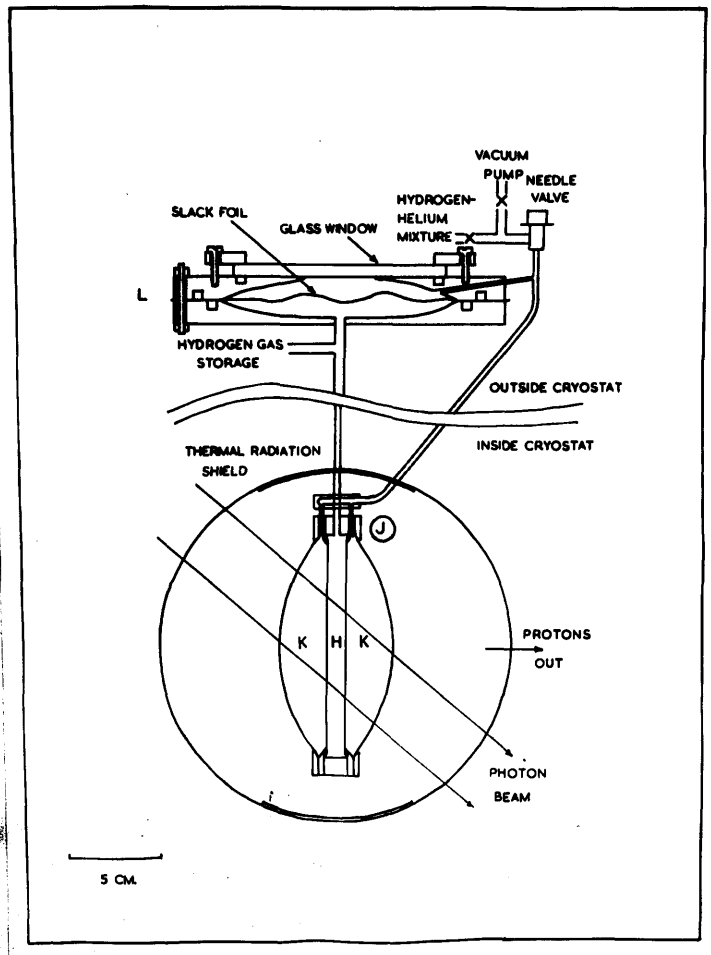
VACUUM
PUMP
NEEDLE
VALVE
HYDROGEN-
HELIUM
MIXTURE
SLACK FOIL
GLASS WINDOW
L
HYDROGEN GAS
STORAGE
OUTSIDE CRYOSTAT
INSIDE CRYOSTAT
THERMAL RADIATION
SHIELD
J
K
H
K
PROTONS
OUT
PHOTON
BEAM
5 CM.

fig. 8

into two chambers with rigid walls on all faces except the common one, which is very flexible and impermeable to gases. If the pressure in the target side varies due to any of the causes mentioned above, the film in the compensator moves, altering the volume of the outer layer system, which is closed off, until its pressure is the same as that of the target, so that the target walls are again flat. This system has been shown to compensate actively for a pressure change of as little as $\pm$ 20$\mu$ Hg. Figure 9 shows its performance during a test at room temperature. The range of compensation is expected to be $20^{\circ}K/300^{\circ}K = {}^{1}/_{15}$ of this in operating conditions. This has been checked by evaporating aluminium onto a wall of the target chamber and observing, with an optical device quantitatively sensitive to departures from flatness, through a hole in the radiation shield. This also showed that the liquid hydrogen did not boil in the target in operating conditions.

The actual thickness was accurately measured using a travelling microscope with a shallow depth of focus. By making use of parallax between the image and eye piece cross wires, it could be set accurately on one wall then racked back to the other with statistical deviation in the difference of the readings of 0.002 cm. Measurements in different positions showed that the target was parallel

walled to within the accuracy of measurement and that its thickness at room temperature was 0.998 cm ± 0.4%. On cooling to liquid hydrogen temperature, a 0.33% contraction was calculated to occur and was allowed for.

The advantages of keeping the target material and refrigerant separate were compensated partially by the disadvantages of having to liquefy the target material in the cryostat. This was done by passing hydrogen gas through activated charcoal traps cooled in liquid nitrogen, then into the cryostat where it was again precooled by nitrogen and then liquefied in coils wound round the hydrogen refrigerant container, to fill the target through a pipe leading into the bottom. This meant that it could be used with almost no modification as a liquid deuterium target.

Mechanically, the target chamber was constructed as in figures 8 and 10. The melinex film walls were all 0.001" thick, though thinner ones could of course have been used for the inner walls. The inner films were sealed onto the flat faces of a copper ring with hot setting Araldite cement. On each side of this was a stepped structure as shown to tension the inner walls by stretching and also, in the thinner targets, to give enough thickness in the central copper ring to allow easy entry of pipes to the target space. On the

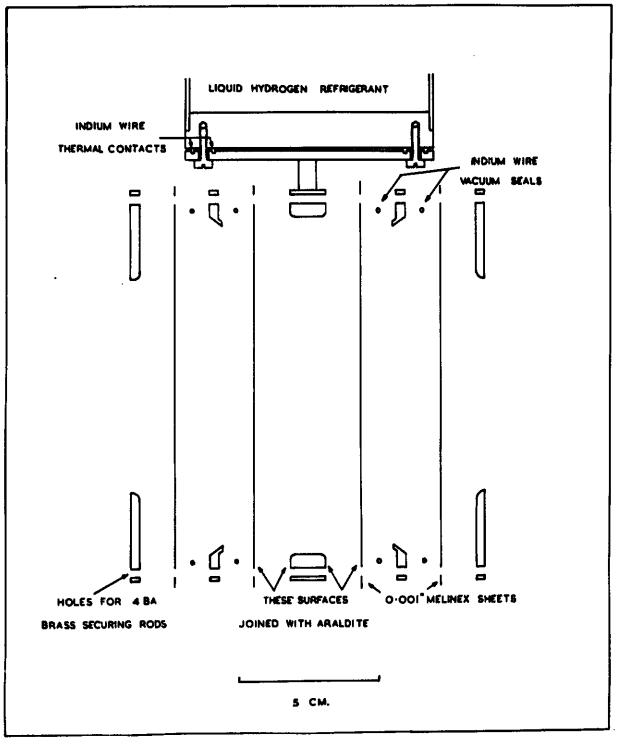
LIQUID HYDROGEN REFRIGERANT
INDIUM WIRE
THERMAL CONTACTS
INDIUM WIRE
VACUUM SEALS
HOLES FOR 4 BA
BRASS SECURING RODS
THESE SURFACES
JOINED WITH ARALDITE
0·001" MELINEX SHEETS
5 CM.

fig. 10

outside of this were other brass plates with large holes with rounded edges which supported the outer beam and particle windows across which there was a pressure difference of 1 atmosphere. The mean thickness of the dense gas in the outer layers was 2.0 cm.

The four outer vacuum seals were made by O-ring gaskets of indium wire and behaved perfectly under repeated temperature and pressure cycling.

During the runs, background measurements were made with the level of liquid hydrogen reduced by boiling off until it was well below the level of the beam. The particles then detected were produced in the walls and in the cold hydrogen gas and helium dilutant. Thus the difference between the target full and target empty counting rates was due to the removal of a layer of liquid hydrogen, 1 cm. thick and replacement with hydrogen gas at the same temperature and pressure. Values for these densities were taken from the tables published by Wooley et al. (1948).

## 5. The Cryostat.

The target chamber is kept cold by contact with a vessel containing liquid hydrogen. Supplies of liquid hydrogen in Glasgow have to be transported by road

200 miles from Liverpool. The inconvenience involved in this arrangement meant that special care had to be taken to reduce the heat input into the cold system to conserve liquid hydrogen.

The cryostat, shown in vertical section in figure 11, was based on standard designs and will be only briefly described here.

The liquid hydrogen refrigerant was contained in a 1 litre cylinder suspended by thin walled low conductivity copper-nickel alloy tubes. A high vacuum ( $< 10^{-6}$ mm. of mercury) was maintained around this system by an oil diffusion pump operating continuously. To reduce radiation heat transfer to the liquid hydrogen, the walls of this enclosure were maintained at $77^{\circ}$K by boiling liquid nitrogen. This liquid nitrogen was enclosed again in an annular cylinder suspended by low conductivity tubes in the high vacuum. The surfaces of the various vessels between which a temperature difference existed were coated with bright aluminium foil of low emissivity to reduce radiant heat transfer.

The part of the thermal radiation shield around the target chamber was of $\frac{1}{16}$" aluminium, with ports cut in it for the passage of the particles and the photon beam. These ports were covered with $\frac{1}{5}$ thou. aluminium foil. The outer vacuum jacket had corresponding large windows of 2 or 4 thou. melinex film.

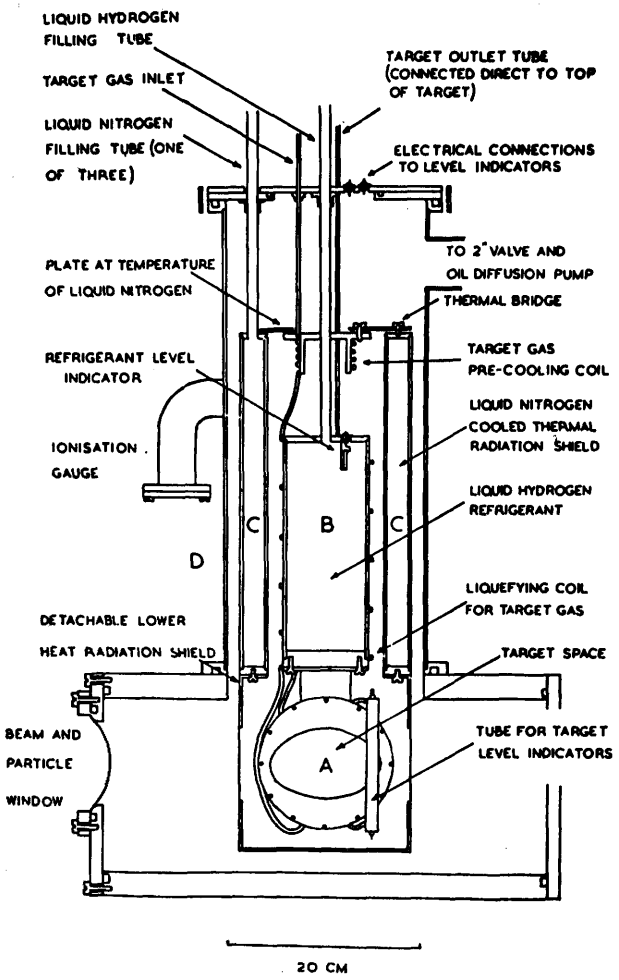


Vertical section through cryostat.

---

fig. 11

During operation, the liquid hydrogen boiled off at the rate of about 1 litre in about 30 hours. Thus it was conveniently refilled from the 16 litre transport and storage dewars once each day. Including losses in transferring and conversion of liquid hydrogen from the ortho - to the para - form, one storage vessel full lasted, on the average, one week.

The losses of liquid nitrogen were larger, and the 3 litre annular cylinder lasted between 5 and 10 hours. A simple, novel control switch was made which automatically refilled this from a large liquid nitrogen storage dewar each time it emptied. This is described in § 7 below.

6. Lining up.

Advantage can be taken of the flat slab nature of this target by setting it at such an angle to the photon beam ( $40^{\circ}$ in this case) that it presents minimum thickness to the particles to be counted and greater thickness to the photon beam ( figure 8.)

For the accuracy needed in this cross-section measurement it was essential to know the position of the centre of the target to a few millimetres and to be able to pass the beam through it and line up the counters to within $\frac{1}{2}^{\circ}$ on it. This was done with the aid of a 22" diameter protractor which fitted round the base of the

vacuum jacket. Accurately concentric circles were drawn on it, and it was marked off every $2^{o}$. Radial arms were attached to this at the angles shown in figure 12, and from these arms plumb lines were dropped. The centre of the target was marked by a cross on its edge and a thin wire was stretched vertically across the face of the target parallel to it and exactly across its centre. This wire, held between two brackets, was out of the photon beam. The flat wall of the target below the wire had been made a mirror by evaporating aluminium on to it during construction and small holes and slots were cut in the radiation shield to view these marks, and also the top and bottom edge of the face of the target.

By moving the protractor relative to the cooled cryostat it was arranged that:-

1. Two plumb lines on the $40^{o}$ arm were in line with the centre of the target and were at right angles to it. ( i.e. The two plumb lines, the vertical wire and their reflections in the mirror were all coincident.)

2. The protractor was moved along the $40^{o}$ line until the two plumb lines on the $50^{o}$ arm were collinear with the cross on the edge of the target. The protractor was now clamped to the cryostat with the

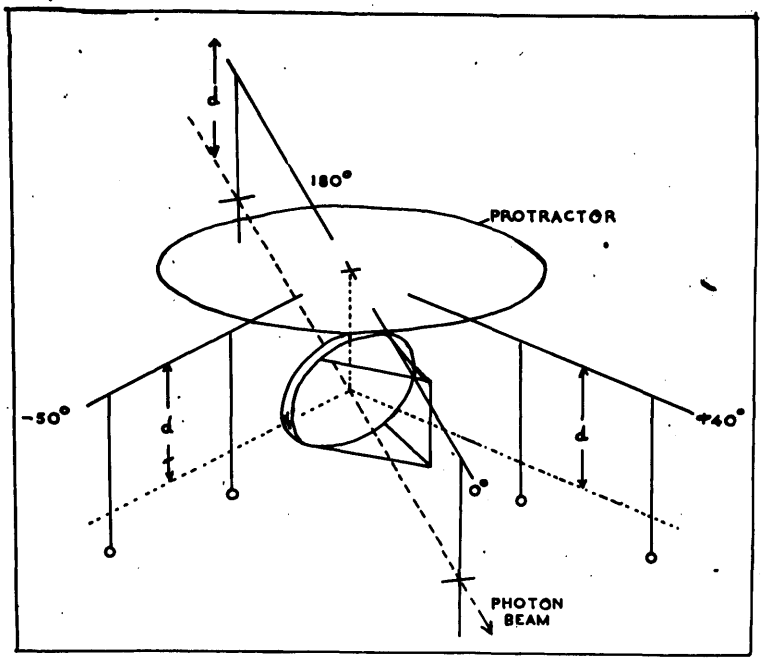


fig. 12

assurance that the centre of the protractor was vertically above the centre of the target.

3. This vertical distance "d" was measured by means of the cross on the edge, and the top and bottom of the face of the target.

4. Metal cross-wires were suspended from the $0^{o}$ and $180^{o}$ arms of the protractor so that a line joining their centres passed through the centre of the target. Photographic plates were placed behind each and exposed to the X-ray beam from the synchrotron. An image of the cross-wires and the beam was developed om the plates and the whole cryostat was moved until the X-ray beam passed in the proper direction through the centre of the target.

## 7. Auxilliary devices.

### Cryostat liquid level indicators.

It was important to have a definite check that the target was full of liquid hydrogen during the runs and that it was empty during background runs. An improved indicator was developed in this laboratory from devices described by Wexler and Corak (1951) and Clement and Quinnel (1952). This consisted of a vertical side tube connected to the target at top and bottom so that the liquid level in it was the same

as in the target. (J in fig. 8 see also fig. 11) This tube contained two 68 Ω carbon resistances, one above beam level, and the other below. These were electrically connected to outside the cryostat where either could be selected to form an arm of a Wheatstone bridge. This was designed in such a way that 0.3 watts was dissipated in the level resistor. When this was in the liquid, this power was rapidly dissipated and the bridge had a stable balance point. When the resistor was in cold gas, the rate of heat dissipation was much less and the resistor warmed up, giving a slow change of resistance and drift of balance point which unambiguously differentiated liquid from gas. The same scheme was used to indicate when the 1 litre hydrogen refrigerant was full.

## Liquid Nitrogen refiller.

For unattended overnight refilling of the liquid nitrogen radiation shield, some automatic device was needed which refilled the reservoir only when it was almost empty. Enquiries and a search of the literature revealed only unnecessarily complicated machines. An elegant and original controller was constructed which did this job. It consisted of two liquid level indicators in the form of bellows vapour pressure thermometers which dipped into the radiation shield. The movements of

these were coupled to a special mercury switch with controlled backlash in such a way that when both sensitive levels were out of liquid, the main nitrogen storage dewar was pressurised with gas by electro-magnetic valves, driving over liquid nitrogen, until both sensitive levels were reimmersed. This has been described in the Journal of Scientific Instruments ( 38, 162 (1961)).

Cryostat vacuum windows.

Initially trouble was experienced with atmospheric water vapour diffusing through the large melinex windows on the vacuum jacket and condensing as frost on the radiation shield. This had the effect of giving a slowly rising background of protons from photodisintegration of the oxygen and also an increased loss of liquid nitrogen due to higher emissivity. For the main runs, this was overcome by making these windows double with a 0.0005" outer window and continuously passing through the interspace a stream of dry nitrogen gas evaporated from the cryostat to sweep out water vapour.

General.

A general description of this target has been published (Bellamy et al. (1960)).

This form of target has proved useful for many

investigations. Besides the work presented in this thesis, it has been used in measurements of the photoproduction of $\pi^+$ mesons near threshold(Rutherglen et al. (1960)) and filled with liquid deuterium it has been used, by H.C. Evans, in an investigation of the "spectator model" of meson photoproduction in deuterium ( to be published). It is now being used to extend the measurements reported here to other angles and energies. Other similar models have been made, the thinnest being 2 mm$_{\text{thick}}$ intended for measurements on elastic $\pi^o$ photoproduction at deuterons by detection of the recoil deuteron.

Further modifications suggest themselves. The wall thickness and density of the surrounding gas layers can be reduced by operating with refrigerant boiling at less than 1 atmosphere pressure, resulting in lower background while retaining the property of arbitrary but precisely known thickness. For some experiments suitable extensions could be provided to remove the outer walls from the sensitive region of the detector.

## Chapter V.

### Particle detection system.

### 1. Introduction.

From the diagram of kinematical relationships shown in figure 13 it is seen that protons to be measured have energies in the range 20 to 60 Mev.

In all experiments with bremsstrahlen a major difficulty is the high flux of electrons and low energy photons issueing from the target due to Compton scattering and pair production processes. Above meson threshold there are also $\pi$ mesons and their decay products. The walls of the target produce, by photodisintegration, a flux of neutrons, protons, deuterons, etc. The estimated number of particles which would be produced into 0.01 steradian at $40^{\circ}$ to the beam by the passage of $10^{9}$ equivalent quanta of energy 300 Mev through the target described above is shown in table 2.

The specification of the counter is that it should be able to separate protons from the rest and measure their energy in an instantaneous counting rate $\sim 5 \times 10^{4}$ per second.

### 2. Identification of protons.

Separation of particles of different mass and energy usually needs measurements of two quantities which differentl

**Table 2.**

| | target empty | target full |
|---|---|---|
| relativistic electrons | $2 \times 10^3$ | $10^4$ |
| mesons | 0.1 | 1 |
| protons 20-30 Mev | 4 | 8 |
| protons 40-50 Mev | 0.2 | 20 |
| deuterons and heavier particles (all energies) | 0·1 | 0·1 |

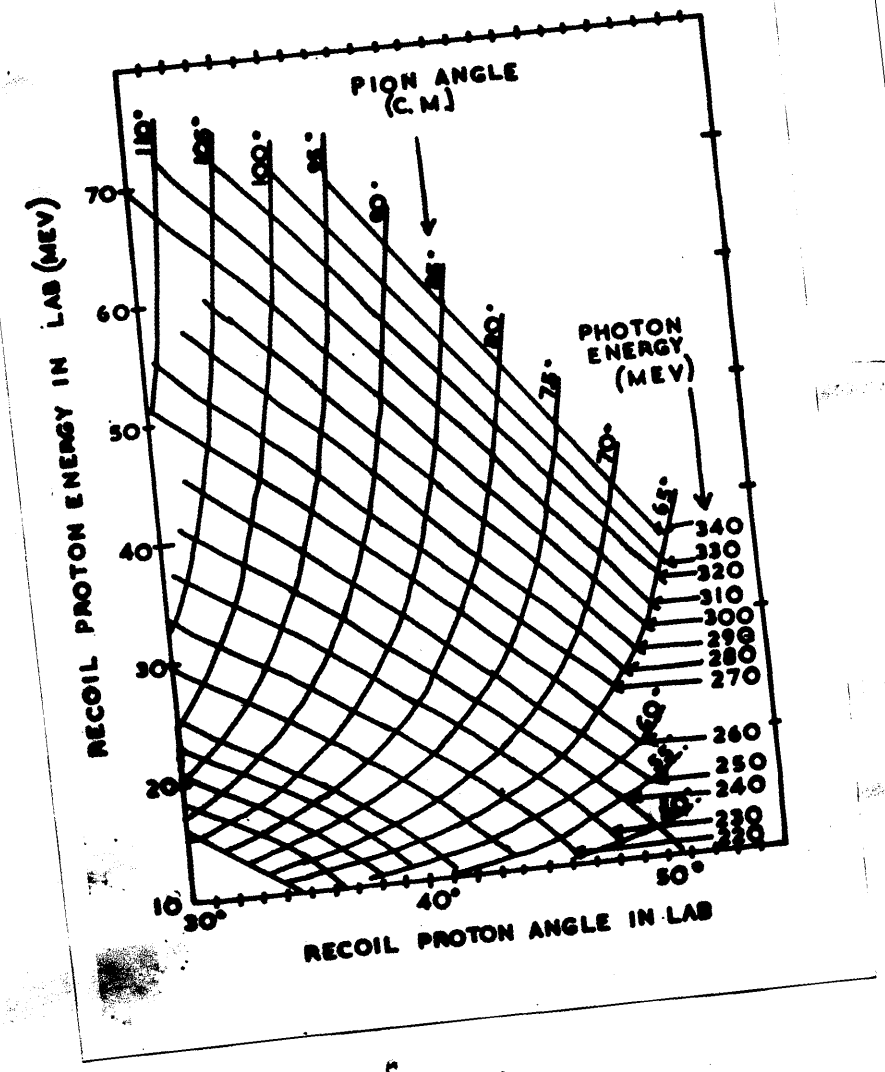
PION ANGLE (C.M.)
PHOTON ENERGY (MEV)
RECOIL PROTON ENERGY IN LAB (MEV)
RECOIL PROTON ANGLE IN LAB
70
60
50
40
30
20
10
30°
40°
50°
340
330
320
310
300
290
280
270
260
250
240
230
220

Fig. 13

involve the mass and velocity of the particle. Measurement of momentum ( by bending in a magnetic field) conveniently cover only a small range of momenta at a time. Direct measurement of range separates into rather coarse energy groups.

dE/dx and V both depend in the same way on mass and velocity so either can be paired with a measurement of energy to perform the separation.

In this case measurement of dE/dx presents difficulties. The dE/dx counter must be thin enough to absorb only a fraction of the energy of a 20 Mev proton. Then when used on higher energy protons, and mesons, a rapid worsening of the resolution is found, due to the lower energy loss and the larger statistical fluctuations in it called the Landau effect. This can be reduced by using a telescope of counters of progressively increasing thickness. The counter(s) immediately in front of the one in which the particle stops being used as a measure of dE/dx.

In view of the difficulties associated with the dE/dx and E technique, it was decided to try the alternative way - measuring velocity and energy. At the beginning of this work fast high gain photomultipliers had just become available. Measurement

of the time interval between the front edges of pulses from counters separated by some distance in a beam of particles would give the time of flight of the particles between the counters and hence the velocity. This does not make such stringent demands on the pulse height resolution in the counters, but a sufficiently large number of photons must be available to drive each photomultiplier to give a minimum variance in the rise time of the pulses.

## 3. Description of Counters.

The fastest suitable photomultiplier available were 14 - stage RCA 6810-A with a transit time spread of about 1 ns. ( $10^{-9}$ seconds). Plastic scintillator (Nuclear Enterprises Ltd. NE102) was selected as the phosphor because of its fast decay time ( about 3 ns.) and being solid was easier to make into thin layers. It was thought possible to obtain a time measurement to an accuracy of $\pm$ 1 ns., so a flight path of 1 metre was chosen to allow of good particle separation while achieving a useful solid angle with a convenient size of counter.

At proton energies $>$ 40 Mev, it again becomes difficult to measure the time of flight over 1 metre accurately enough to achieve good particle separation.

So up to 40 Mev the protons stopped in counter number 2 and the time of flight was measured between counters 1 and 2. ( See figure 14). Between 40 and 65 Mev, the protons penetrate counter 2 and stop in counter 3. The pulse heights from these counters give approximate measures of "dE/dx" and "E" which give good separation in this range.

The planar scintillators were arranged normal to a straight line through their centres. This axis pointed towards the centre of the target and its angle to the incident beam was measured on the protractor described previously.

Counter no. 1 was made from a block of NE 102 hot pressed to 0.020" thick. It's sensitive area was a rectangle 9 cm. x 7.5 cm. 96 cm. behind this was counter no. 2. This was $\frac{1}{2}$" thick and a 5" x 3" rectangle. Counter no. 3 was about 1 cm. behind this again and was a 6" x 4" x $\frac{3}{4}$" thick block which overlapped no.2 all round its edge. The scintillators were shielded by two layers of 0.0002" aluminium foil and perspex light guides packed in magnesium oxide powder conveyed the light to the $1\frac{1}{8}$" diameter photocathodes. The space between the vacuum window of the target and the front scintillator was 20 cm. of air; the 1 metre flight

path was contained in a thin walled box containing hydrogen gas which was continually flushed out by the gas boiling off from the cryostat.

The solid angle and angular resolution were defined by counter no. 2, which was specially mounted to give a clearly defined active area. The size of the scintillator was 7.61 cm. x 12.75 cm. and the distance from the centre of the target to its front face was 142.3 cm. for measurements at $36^{\circ}$ and 142.9 cm. for $40.5^{\circ}$ to the photon beam. This gives an angular resolution function $3^{\circ}$ wide at half height. The solid angle is 0.00479 sterad. at $36^{\circ}$ and 0.00475 sterad. at $40.5^{\circ}$. The errors in these measurements, and the variation of solid angle over the target and the variation for different proton energies total $< 1\%$.

Thick lead shielding was provided as indicated in figure 14 to protect against radiation other than from the target. It was positioned to minimise scattering - in of particles.

The size of counter no. 1 was such that the surface joining the extreme edges of the active area of the target to the edges of scintillator no. 2 everywhere cut scintillator no. 1 at least 1.5 cm. from the edge. Calculations of multiple scattering were made(Fermi (1950)).

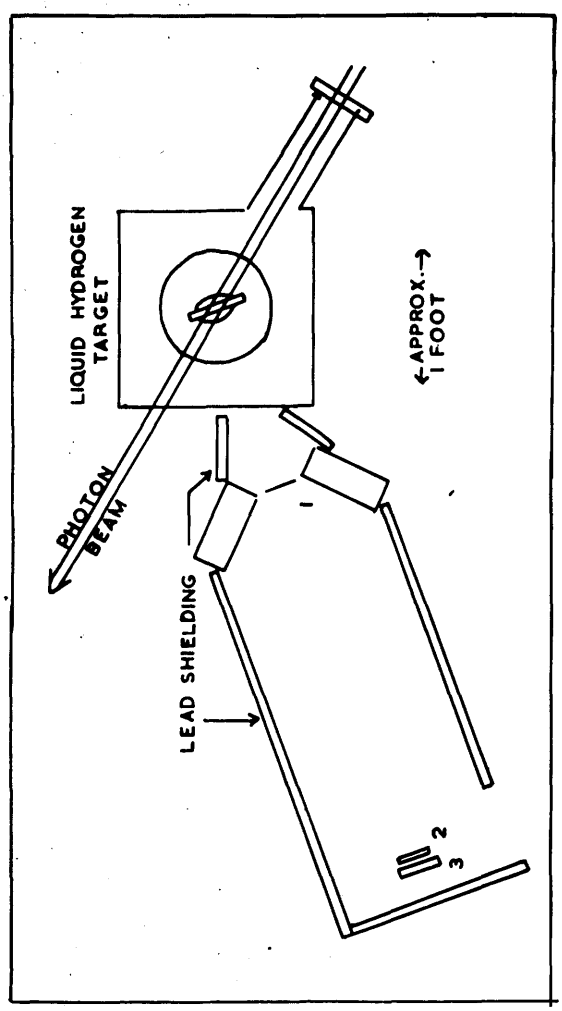
LIQUID HYDROGEN TARGET
PHOTON BEAM
LEAD SHIELDING
APPROX. 1 FOOT
2
3

fig. 14

This is greatest for low energy protons. For 20 Mev recoil protons, the minimum energy is 16 Mev when it reaches the front scintillator. The r.m.s. angle of multiple scattering in this counter was calculated to be $0.7^{o}$. This is sufficient to cause some loss of protons at the edge, but the wide overlap of no. 1. compensates this to some extent by scattering-in , at the expense of a slight loss of angular resolution. The remaining effect is estimated to be $\sim$ 4% for 20 Mev falling rapidly to $<$ 1% for about 30 Mev and above.

Multiple scattering in the 1 cm. liquid hydrogen target is $< 0.1^{o}$ for 15 Mev protons and is negligible as is scattering in other objects in the particle path.

Special care was taken in the design and construction of counters 2 and 3 to get maximum uniformity of light collection and sharpness of energy resolution. It was for this reason that the rectangular parallelepiped shape was chosen ( Brini et al. (1955)). It was also found ( D.Leith, private communication) that the photomultipliers used showed non-linearity ( $>$ 1%) of pulse output with respect to light input if the output current exceeded 3 ma. These aspects were checked using 14.8 Mev protons from the D( $He_3$, $He_4$)P reaction on an

H.T. set and the Compton edges of the 2.6 Mev Thorium and 1.28 Mev $Na^{22}$ $\gamma$-rays. In spite of these efforts an extreme difference of pulse height of 8% was found over different ports of the scintillators. The full width at half height of the resolution curve for 14 Mev protons was about 18%.

4. Time of flight measurement.

The time of flight was measured in a circuit (figure 15) based on that of Azuma and Lewis (1957). A fast negative pulse from the anode of photomultiplier no. 1 was used to cut off a standing current of about 60 ma. in a pair of E 180 F valves in parallel. The common anode load of these valves consisted of a 200 $\Omega$ resistance in parallel with a 200 $\Omega$ impedance output cable (Transradio C3 - T). A sharply rising 6 volt positive pulse was transmitted along the length of this cable until it was reflected from the shorted end back to the terminating resistor. The cable was tapped off at 4.5 metres from the shorted end. At this point a fast ( $\lesssim$ 4 ns.) rising and falling pulse about 6 volts high and 30 ns. long was available. Counters no. 1 and 2 each fed one of these pulse limiting and clipping circuits.

The measurement of time interval is made between the rising edge of one pulse and the falling edge of the

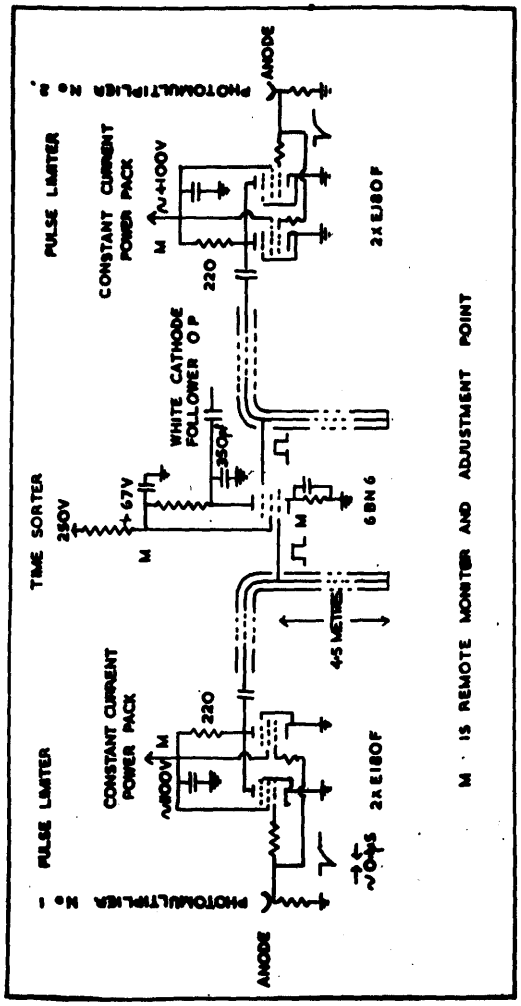
PHOTOMULTIPLIER No. 2
ANODE
PULSE LIMITER
CONSTANT CURRENT POWER PACK
M
~1400V
220
2N EIBOF
WHITE CATHODE FOLLOWER O P
350pF
TIME SORTER
250V
+67V
M
6BN6
4·5 METRES
220
CONSTANT CURRENT POWER PACK
~800V
M
PULSE LIMITER
2N EIBOF
~0·4μs
PHOTOMULTIPLIER No. 1
ANODE
M · IS REMOTE MONITOR AND ADJUSTMENT POINT

fig. 15

other. They were applied to the two control electrodes of a 6 B N 6 gated beam valve. These were ~~normally~~ biassed so that current normally flowed to the "accelerator" electrode of the valve, not the anode. During the short interval (length dependent on the relative delays of the two pulses) during which both grids were pulsed on, a standard current ( almost independent of the heights of the grid pulses, if large enough) was switched from the accelerator to the anode. This current was integrated in a condenser and the voltage change on this condenser was the measure of the time of flight of the particles.

It was advantageous to choose the relative delays (due to transit time in photomultipliers, E180F valves, between the control grids of the 6BN6, and the lengths of the two cables between the E180F limiters and the 6BN6) so that the relative delays were adjusted to give zero overlap for relativistic particles. This cut down dead time and noise in the circuit. The operation of the time measuring apparatus is illustrated in figure 16.

The initial adjustment of this apparatus was made using radioactive sources and cosmic ray μ-mesons. The transit time spread was minimised by raising the voltage between the photomultiplier cathode and first dynode and between the first and second dynodes to its maximum allowed

| | FORM OF PULSES AT GBNG TIME SORTER |
|---|---|
| RELATIVISTIC PARTICLES | COUNTER 1 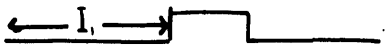  COUNTER 2   GBNG ANODE  |
| FAST PROTONS | 1 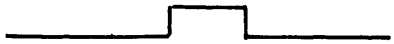 2   GBNG ANODE  |
| SLOW PROTONS | 1 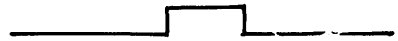 2 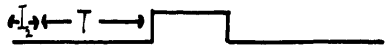  GBNG ANODE  |

fig. 16

$I_1$ = DELAY IN COUNTER ONE SIDE

$I_2$ = " " " TWO "

T = TIME OF FLIGHT

( a very slow particle would again give a small output pulse, but its range is insufficient to reach counter TWO )

value. With small blocks of scintillator and almost no background radiation a resolving time (full width at half height of the time pulse height distribution) of 0.6 ns. was obtained.

Under actual running conditions, the scintillators were much larger in area but thinner, giving poorer light collection, and there was a heavy background of small pulses due to electrons. To reduce the effect of this and achieve optimum working conditions, the following procedure was adopted.

The 20 thou. plastic scintillator was replaced by one of the same shape and area, but 2mm. thick. This was chosen so that relativistic electrons penetrating it gave the same size of light signal as 50 Mev protons in the 20 thou. scintillator. The photomultiplier voltages were chosen to cut off the limiters sharply with single electrons in counters 1 and 2, and the limiter currents to give 6 volt pulses on the 6BN6 grids which were biassed off to - 3 volts. The telescope was set up at $45^{\circ}$ to a thin target in the beam. The delay cable lengths were chosen so that relativistic electrons from this target gave timing pulses with about 50% overlap at the 6BN6. The 6BN6 output was amplified and displayed on a 100 channel kicksorter, in the form of a peak corresponding to particles with the speed of light.

The position and width of this peak was measured as a function of the three variables of 6BN6 grid bias, and the currents in the two limiter circuits. These were varied until the best resolution was obtained with optimum pulse height on the 6BN6 grids. Then keeping these fixed, each photomultiplier H.T. voltage was in turn reduced in small steps and a plot drawn of timing pulse height against photomultiplier voltage. This was at first nearly a straight line (with a slope due to the photomultiplier transit time varying with interstage voltage) but below a certain voltage it exhibited a sharp break downwards, because, with that photomultiplier gain, relativistic particles were no longer cutting off the limiter sharply. Just above this break was taken to be the operating voltage of each photomultiplier, ensuring that the extreme proton energies would operate the device properly. In the case of the front counter, which is exposed to a high flux of electrons, this also ensures that with the thin scintillator in position fast electrons do not operate the limiter, cutting down the random coincidences and dead time.

Having fixed all the operating voltages and currents, the time sorter was calibrated by varying the lengths of delay lines between each limiter and the

6BN6. Knowing the speed of pulses in the cable (0.96 of the speed of light) a straight line calibration was drawn of time delay against pulse height referred to the standard pulse height obtained by connecting both 6BN6 grids simultaneously to counter no.2("full overlap pulse height"). From this line the operational lengths of delay cables for counters 1 and 2 were chosen, according to the criteria given above.

## 5. Electronics.

A block diagram of the electronics is shown in figure 17. The counter telescope and the parts shown within the dotted lines were situated in the synchrotron beam room. The signals were sent via White cathode followers and 70 $\Omega$ cable to a shielded room some 30 feet away, which also contained the power supplies. Monitor voltages from various points were also led to here.

The main amplifiers were commercial wide band amplifiers feeding blocking oscillator discriminators and diode coincidence circuits. The three signals to be measured ( Time (T), counter 2 pulse height ($E_2$) and counter 3 ($E_3$)) were delayed by different amounts and added in a mixer feeding through more delay into a Tektronix oscilloscope type 545 with the sweep triggered

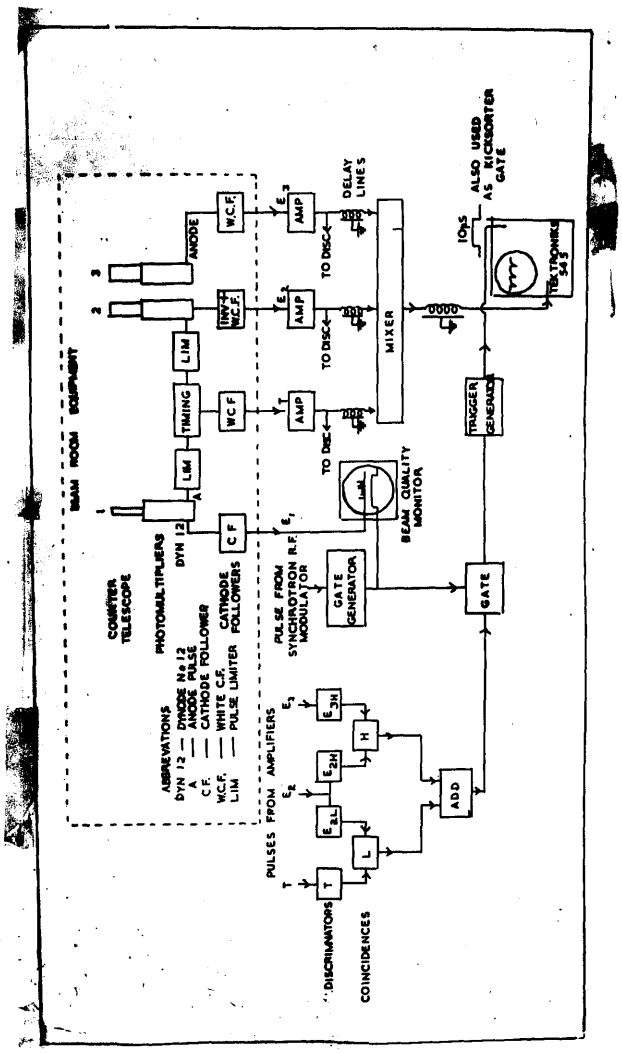
BEAM ROOM EQUIPMENT
COUNTER TELESCOPE
PHOTOMULTIPLIERS
DYN 12
ANODE
W.C.F.
AMP
DELAY LINES
TO DISC.
MIXER
ALSO USED AS DISCRIMINATOR GATE
TEKTRONIX 545
TIMING
LIM
WCF
CF
CATHODE FOLLOWERS
BEAM QUALITY MONITOR
TRIGGER GENERATOR
GATE
GATE GENERATOR
PULSE FROM SYNCHROTRON R.F. MODULATOR
PULSES FROM AMPLIFIERS
DISCRIMINATORS
COINCIDENCES
ADD
ABBREVIATIONS
DYN 12 — DYNODE No 12
A — ANODE PULSE
C.F. — CATHODE FOLLOWER
W.C.F. — WHITE C.F.
LIM — PULSE LIMITER

fig. 17

by either coincidence circuit through a gate which opened about 1 ms. before the X-ray beam pulse began and closed about 1 ms. after it finished. This reduced cosmic ray background and eliminated electrical pickup from the ignitron switches and high voltage injector of the synchrotron. The oscilloscope traces were photographed by a 35 mm. film camera moved on between each trigger.

## 6. Stability.

Because of the long running time of the experiment (5 weeks) and the fineness of the separation, stability was at a premium. Where possible the characteristics of the apparatus were made to depend on reliable components such as high stability resistors. Where this was not possible, as in the D.C. circuits in the time measurements, facilities for continuously monitoring and correcting important quantities were incorporated.

Before each days run, and at least once more during the day, the characteristics of the whole apparatus were checked. The gains of the energy measuring channels $E_2$ and $E_3$ were checked by displaying on a kicksorter Thorium $\gamma$ ray spectra ( amplified by X 10), and measuring the height of the 2.39 Mev edge. By gating this kicksorter with the oscilloscope trigger, the stability of the T, $E_{2L}$ , $E_{2H}$ and $E_{3H}$ discriminators were

checked by the low cut-offs on the spectra. The timing circuits were partially checked by connecting both 6BN6 grids in turn to the limiters of counters 2 and 1 and displaying the full overlap pulses on the kicksorter. The gain of the oscilloscope was checked by putting these standard height pulses onto the screen and measuring their height. After initial difficulties satisfactory stability was maintained throughout the experiment.

## 7. Calibration and measurement.

The photographs of sweeps on the oscilloscope (e.g. figure 18) were projected onto graph paper with a magnification $\sim$ x 20 and the heights of each pulse were measured. If the sweep showed no pulse due to counter 3, e.g. (a) in figure 18, corresponding to a particle stopping in counter 2, then a spot corresponding to it was plotted on a graph with ordinate of time of flight and abscissa of counter 2 pulse height. A plot of a typical run is shown in figure 19 (a). The theoretical loci , calculated from calibrations described below are shown as dashed lines up to 39 Mev for protons and corresponding energies for other particles. For particles greater than these energies, the particles penetrate into counter 3, losing smaller energy in counter 2 without much change in the time of flight, giving the

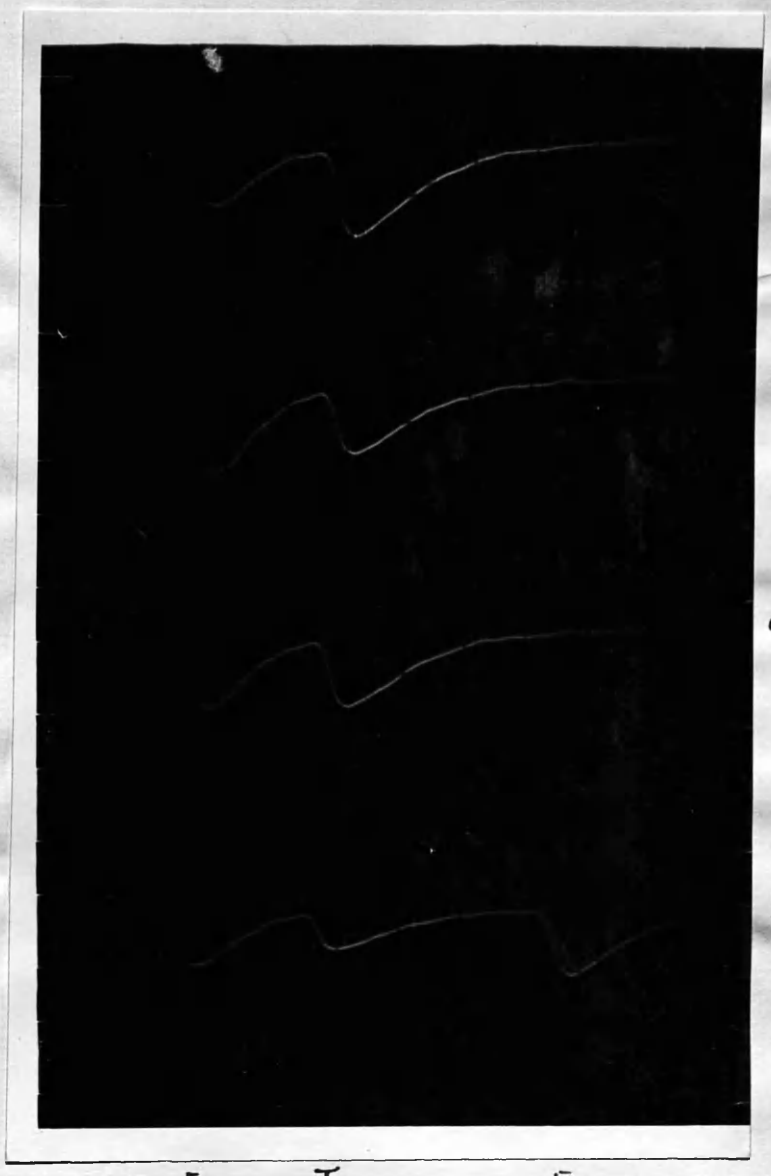


fig. 18

dotted portions of the loci. To avoid confusion, particles with a pulse in counter 3 were plotted on another graph shown in figure 19 (b). In this the horizontal ordinate is still counter 2 pulse height, and counter 3 is plotted vertically down. This is an approximate plot of dE/dx and E. Again the theoretical loci are shown as dashed lines with a break corresponding to penetration of counter 3. This time the break is so far from the energies of interest that ambiguities are not caused.

The positions of the theoretical loci were derived from two sources. The initial calibration was done in terms of the Compton recoil electron spectrum of thorium γ-rays in the plastic scintillator. A calibration of the response of this scintillator for protons relative to Compton electrons has been done by Evans and Bellamy (1960) and Gooding and Pugh (1960). They interpreted their results with a theory which allowed extrapolation to higher energies and other particles. A calibration accurate to about ± 4% was calculated from this, but the final calibration was done with the aid of the pulse heights corresponding to the breaks in the loci. These occur at an energy predictable from range measurements. Values of ranges in plastic scintillator ( approximate formula $CH_{1.1}$) were calculated from the

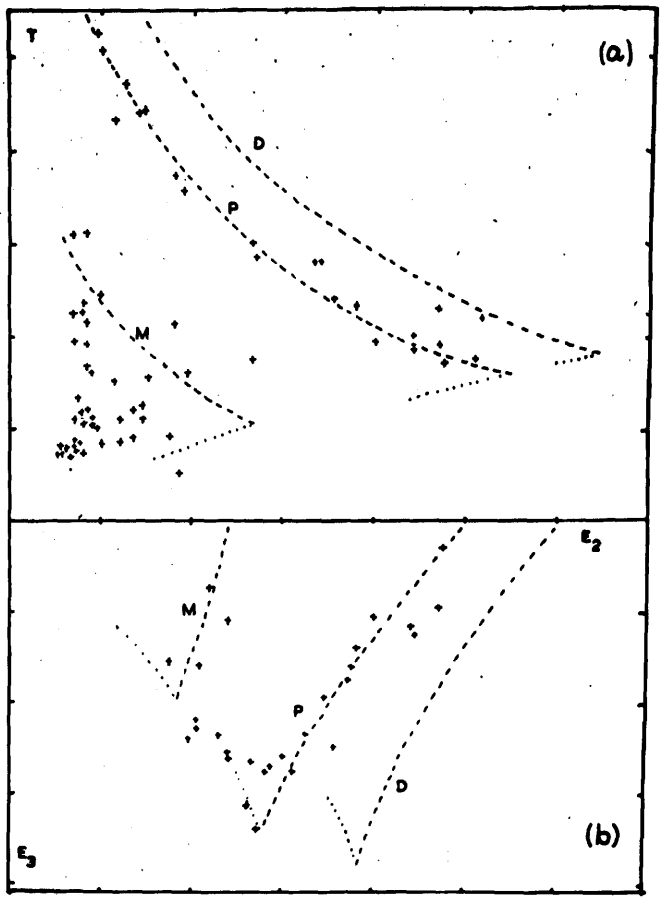


fig. 19

range-energy tables of Rich and Madey (1954). These values were considered accurate for protons to ± 2% and an energy scale was constructed by inserting these values into the equations of Evans and Bellamy.

8. Fast display unit.

The final check of the proper working of the counting apparatus each day was that when plotted as above, the particles lay in about the usual numbers along the right loci. The analysis of each run to this stage was a slow process lasting about 4 hours, during which time, new faults or drifts could occur. To keep a faster check on this, and also to reduce the work in the final analysis, it was decided to do the plotting of the graphs electronically .

The principle of operation was as follows. If the counter pulses were such that the particle could be a high energy proton ( i.e. discriminators $E_{3H}$ and $E_{2H}$ fire, also $E_{2L}$ and possibly T), then a 5μs gating pulse was sent to the controlling terminals of gated pulse lengtheners marked $E_3$ and ( through an adding circuit) $E_2$ and an anti-coincidence circuit suppressed any operation of lengthener T. (see figure 20). When the counter pulses indicated a possibility of being a low energy proton ( i.e. T and $E_{2L}$ discriminators fire; possibly $E_{2H}$ but not $E_{3H}$ ), then the lengtheners T and $E_2$

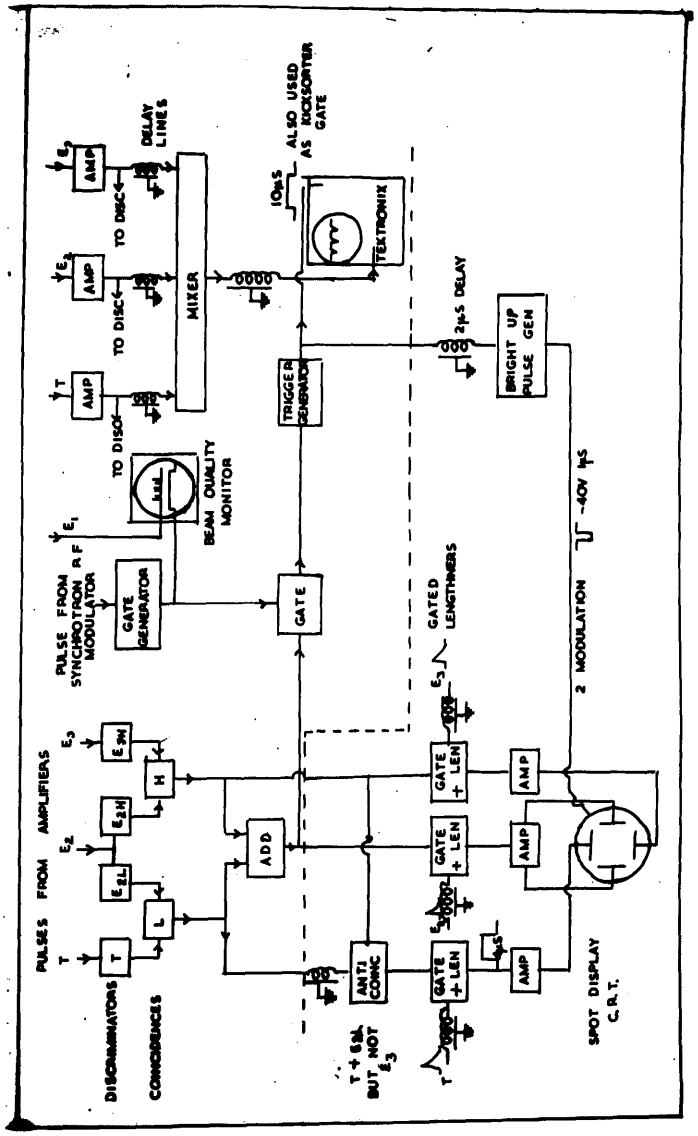
PULSES FROM AMPLIFIERS
DISCRIMINATORS
COINCIDENCES
ADD
ANTI COINC
T + E3 BUT NOT E3
PULSE FROM SYNCHROTRON RF MODULATOR
GATE GENERATOR
BEAM QUALITY MONITOR
MIXER
DELAY LINES
TO DISC
AMP
TRIGGER GENERATOR
GATE
GATED LENGTHNERS
GATE + LEN
ALSO USED AS KICKSORTER GATE
TEKTRONIX
2μs DELAY
BRIGHT UP PULSE GEN
2 MODULATION
-40V
SPOT DISPLAY C.R.T.

fig. 20

were operated, but not $E_3$.

These gated lengtheners had the property that when no control pulse was applied, no output was produced. If an operating pulse was applied, then the output followed any pulse also applied at the input to its maximum voltage, then when the input fell again, the output stayed at thepeak level of the input until the control pulse was over, and then returned to zero.

The inputs to these lengthening gates were derived from the main amplifiers via delay lines of length sufficient to ensure that the gate was fully opened before the peak input pulse was reached, so that ~~the~~ lengthening to the peak height was obtained. The square 4μs long pulse outputs of the lengtheners were amplified by a single stage of amplification, and, following a suggestion by Dr. D.T. Stewart, were applied to the plates of a Cossor double beam cathode ray tube. The $E_2$ pulse was applied to the X plates, and the T and $E_3$ pulses to the $Y_1$ and $Y_2$ plates respectively. The brightness of the oscilloscope was normally very low and the spot stationary, but whenever a low or high energy coincidence took place (during the synchrotron X-ray beam pulse) a 1 μs wide pulse, derived via a 2 μs delay from the Tektronix oscilloscope trigger/kicksorter gate - generator, was applied to the cathode ray tube brightening

up the spot. The relative delays were so chosen that this occured when the voltages on the deflecting plates had reached a steady value corresponding to the peak height of the pulses in the appropriate channels, so two fine spots were formed on the screen. Because of the coincidence - anticoincidence arrangement for triggering the lengtheners, only one spot at a time was deflected in the Y direction, although both were deflected in the X direction. Thus the graphs of figure 19 were plotted on the cathode ray tube screen.

The screen was photographed on 35 mm. film and typical examples showing the protons, mesons, deuterons and randoms are shown in figure 21. These pictures provided a fast ( about 15 minutes delay) visual check on the proper operation of the apparatus.

Analysis was carried out by projecting the film through the same optical system as was used for the individual oscilloscope sweeps. The two lines traced out by the spots not deflected in the Y directions and the two spots made by the low D.C. brightness of the undeflected spots were used as fiducial marks. The theoretical loci were transferred on to this projection and fixed bands were drawn and used to classify the spots into definite protons, definite non-protons and uncertain particles according to which band they lay in.

fig. 21

The description of the further analysis is deferred to Chapter VI.

All the experimental runs were recorded on this display of spots. For at least several hours each day both this system and the previously described slower system of photography of counter pulses on individual oscilloscope traces were used simultaneously. These were analysed and the individual particles correlated in the two forms of the display and by correlating the pulse height measured on the oscilloscope traces with the corresponding coordinates measured in the projected spot pictures, analyses such as are shown infigure 22 were obtained. The non-zero intercepts on the axes of this correlation are due to the action of the lengtheners which produce a negative pedestal $\sim$ - 1 volts when triggered. These correlations provided proof of the linearity and stability of the electronics and allowed transfer of the theoretical loci and the use with confidence of the spot display for final analysis.

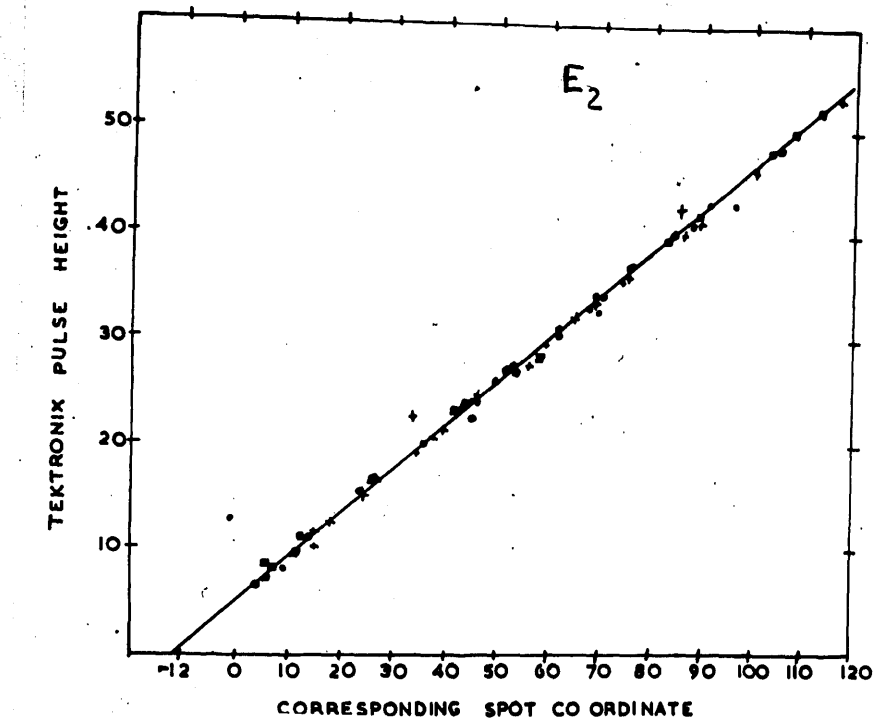
$E_2$
TEKTRONIX PULSE HEIGHT
10
20
30
40
50
-12
0
10
20
30
40
50
60
70
80
90
100
110
120
CORRESPONDING SPOT CO ORDINATE

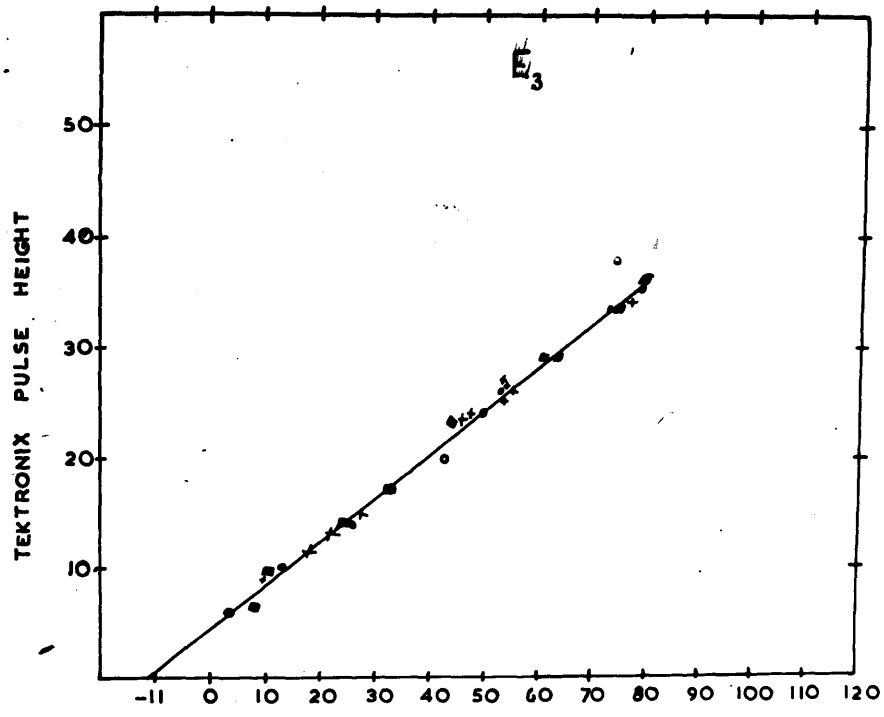
$E_3$
TEKTRONIX PULSE HEIGHT
10
20
30
40
50
-11
0
10
20
30
40
50
60
70
80
90
100
110
120

fig. 22

## Chapter VI.

Performance of the experiment and analysis of results.

### 1. Performance.

Measurements were made on 17 days extending over a synchrotron run of about 5 weeks. Individual runs, each of about $10^{10}$ equivalent quanta with about 100 proton counts of all energies, lasted between 5 minutes and 30 minutes. Runs were done first with the target full at $36^{\circ}$ and then $40.5^{\circ}$. Then the target was emptied and background measured at $40.5^{\circ}$ and $36^{\circ}$. The quality of the photon beam (length, position with respect to peak field, and intensity distribution in time) was monitored continuously and any runs in which it did not fulfil the conditions stated in chapter 3 were discarded before analysis.

### 2. Analysis.

The photographs of the spot displays of the remaining runs were projected as described in chapter V and the definite protons and doubtful spots counted separately into groups or bins of different energies, each about 3 spot diameters wide. There were 70 bins for the low energy protons and 60 for the high energy.

The integrated photon flux was calculated for

each run, corrections being applied for the drift of the integrator zero point and the variation in atmospheric density.

3. Dead time corrections.

An average photon intensity was calculated for each run. The runs were grouped according to whether the target was full of liquid hydrogen or empty and by each of the two recoil angles of protons observed and further divided into low, medium and high intensity runs according to the average photon intensity. In each sub-division the number of protons was found in a region not including discriminator thresholds, and the average number per unit of integrator flux was plotted against the mean photon intensity. It was found that within the statistical accuracy ( about 3%) the protons per unit of flux was independent of photon intensity, showing that the counter dead time correction is small.

Another estimate of the dead time was made from the dead time of the discriminators and an estimate of the mean instantaneous counting rate. When applied to the runs with full target this gave a correction of 1.2% to the proton numbers, but because of uncertainties in the counting rates, length of beam and dead time to be associated with the timing circuit, this is probably 1.2% $\pm$ 1.2%. The correction to be applied to the

target empty runs will be about 5 times smaller than this ( because of the lower counting rate) and was ignored.

The total photon flux ( embodying the corrections for dead time) was calculated for the two conditions of target full and target empty for each of the two angles of observation.

4. Counter resolution.

In spite of the rapidly rising cross-sections the observed proton spectra are not steeply rising. This is due to a combination of factors due to the reaction kinematics, smaller number of high energy photons and non-linear proton energy calibration. Estimates were made of the correction to be applied to the observed spectra to allow for the finite counter resolution and its variation with energy. Except near the end points of the particle loci these were small and no corrections were made.

The high energy end point cut offs have a slope corresponding to a resolution $\sim$ 9% full width at half height. This is chiefly made up of non-uniformity in light collection in the counters , a Landau spread ( $\sim$ 4%) in light emission from the scintillators for protons of a given range, and variation in the discriminator

level in counter 3.

5. Background subtraction.

The proton spectra of the target empty runs were normalised to the same photon flux as the corresponding target full runs. With the target full, half the background has to penetrate 1 cm. of liquid hydrogen. The number in each background bin was halved and one half was shifted down in energy by a calculated amount, depending on the energy, to account for the spectrum distortion on filling the target. The two halves were then added, and the total subtracted from the target full runs.

It should be noted that some part of the uncertainty of identification of particles as protons is eliminated by background subtraction. Uncertain particles which are incompletely distinguished deuterons, tritons, alphas etc. as well as $\pi^-$ mesons from the walls producing stars in the counters are largely eliminated. No account has been taken of this in the final estimation of errors.

6. Energy spectrum, correction for energy loss in the target.

This procedure yielded the proton spectra from liquid hydrogen for two lab. angles. Each spectrum consisted of a low and high energy part and energy

calibrations (calculated as described in chapter V § 7 and 8) were made for protons recoiling from both the extreme front and back faces of the target. ~~were made.~~ Using the equal probability for production at any depth in the target and neglecting the small variation of dE/dx in the target for recoiling protons, these spectra in terms of coordinates of displayed spots were converted to those of true recoil energy with a bin width of 1 Mev.

The low energy spectra limits were 21 Mev and 36 Mev, and thehigh energy spectra 45 and 55 Mev.

The low energy protons above 36 Mev and the high energy protons below 45 Mev were added together into bins of 9 Mev width, because of uncertainties arising from the background spectrum change on filling the target, the variation of energy loss with depth in the full target and the nearness of the end points of the particle loci.

The total corrected number of protons in each 1 Mev bin was about 100 at 20 Mev rising to $> 200$ at higher energies.

## 7. Calculation of cross-sections.

Each bin at each angle was transformed to a cross-section in the centre of mass using appropriate averages,

over the laboratory angular width, of the photon density and kinematical factor d $\cos\Theta^*$ /d cos $\Theta$ . (Taken from the tables of Malmberg and Koester (1953). These are calculated for a $\pi^o$ mass of 136.0 Mev. The use of the now accepted value of 135.04 Mev produces negligible changes in this energy region) . These cross-sections correspond to angles between $78^o$ and $98^o$ for $\pi^o$ emission in the centre of mass system , averaged over a photon energy interval determined chiefly by the angular width of the counters. Small corrections (always $<$ 4% for $36^o$ measurements and $<$ 10% for $40.5^o$ and averaging much less) taken from previous measurements of the angular distributions (see chapter 2, figure 1 ) were applied to these to convert them to $90^o$ in the c.m. system.

The 1 Mev bins were then grouped together to give the best combination of statistical accuracy and narrowness of range of $E_\gamma$. The results are shown in Table 3 and figure 23. The limits of uncertainties shown refer to the relative sizes of cross-sections and derive chiefly from the statistical uncertainty in the number of protons in each energy bin (allowing for background normalisation and subtraction) but also include the uncertainty of identification of particles as protons and the effects of

multiple scattering in the front counter and p - p scattering in counters 2 and 3. Also included are

1. solid angle variation with energy and uncertainty in changing from $36^{\circ}$ to $40.5^{\circ}$ - 1%.
2. relative numbers of photons 1% between 200 and 270 Mev rising to 1.5% at 280 Mev 2.5% at 290 Mev 4% at 300 Mev.
3. Uncertainty in conversion factor from lab.system to centre of mass system and uncertainty in correction from observed angle in centre of mass system to $90^{\circ}$ in the centre of mass system - variable over energy range ( $<$ 1% at the high proton energies rising at low energies to 3% at $36^{\circ}$ and 5% at $40.5^{\circ}$)

The values of the table, regarded as absolute contain, in addition to the above uncertainties the following which affect them all in the same way.

1. absolute calibration of Cornell chamber $\pm$ 3%.
2. absolute calibration of ion current integrator 0.5
3. uncertainty in correction factor for absorbtion by material in the path of the beam 0.5% .
4. thickness of target 0.3%.
5. density of liquid hydrogen and vapour 0.2%
6. counter dead time correction 1.2%.

Giving a total of $\pm$ 3.3%.

8. Other corrections.

In all the above it is assumed that recoil protons are produced only by the photoproduction of $\pi^o$ mesons (background subtracted). The processes which are most likely to be confused are :—

1. Elastic scattering of high energy photons by protons. This has been measured in the relevant energy range by Bernardini et al. (1960) and De Wire et al. (1961). The cross-section in the centre of mass system is about 1% of that of $\pi^o$ photoproduction.

2. Elastic scattering of fast neutrons.

These originate in the synchrotron target and collimator (which has a transmission of only about 10%). An estimation of this shows that with the shielding used it is negligible.

3. Photodisintegration of deuterium.

Natural hydrogen contains about 1 part in 6000 of deuterium. The photodisintegration cross-section is $\sim$ 10μb/sterad for proton energies of interest (Whalin et al. (1956)) which gives a correction $\ll$ 1%. No other impurities should exist in the liquid hydrogen.

No corrections have been applied for any of the above.

Table 3.

Results of measurements.

A Measurements at 36° in laboratory.

| Median γ ray energy | Eγ range (Mev) | $\frac{d\sigma}{d\Omega}$ c.m. μb/sterad | correction to 90°c.m. | A μb/sterad | total relativ uncerta inty |
|---|---|---|---|---|---|
| 209 | 203 - 215 | 2.99 | +0.13 | 3.12 | ± 0.56 |
| 215.5 | 208 - 223 | 3.64 | +0.09 | 3.73 | ± 0.41 |
| 222 | 216 - 228 | 4.13 | +0.02 | 4.15 | ± 0.54 |
| 226.5 | 220 - 233 | 4.82 | -0.03 | 4.79 | ± 0.57 |
| 232 | 226 - 238 | 5.63 | -0.07 | 5.56 | ± 0.56 |
| 236.5 | 230 - 243 | 6.14 | -0.10 | 6.04 | ± 0.54 |
| 243.5 | 236 - 249 | 6.43 | -0.13 | 6.30 | ± 0.57 |
| 256 | 246 - 266 | 10.31 | -0.15 | 10.16 | ± 0.30 |
| 270.5 | 263 - 278 | 13.54 | -0.13 | 13.41 | ± 0.80 |
| 275 | 267 - 283 | 15.74 | -0.10 | 15.64 | ± 0.86 |
| 279.5 | 272 - 287 | 16.38 | -0.08 | 16.30 | ± 0.90 |
| 285 | 277 - 293 | 18.33 | -0.04 | 18.29 | ± 1.06 |
| 290 | 282 - 298 | 21.68 | +0.00 | 21.68 | ± 1.30 |

Table 3 (continued)

B measurements at 40.5° in laboratory.

| Median $\gamma$ ray energy | $E\gamma$ range (Mev) | $\frac{d\sigma}{d\Omega}$ c.m. μb/sterad | correction to 90° c.m. | A μb/sterad | total relativ uncerta inty |
|---|---|---|---|---|---|
| 227.5 | 220 - 235 | 4.47 | +0.56 | 5.03 | ±0.70 |
| 232.5 | 225 - 240 | 4.31 | +0.49 | 4.80 | ±0.72 |
| 238.5 | 230 - 247 | 5.27 | +0.41 | 5.68 | ±0.71 |
| 244.5 | 236 - 253 | 6.47 | +0.39 | 6.86 | ±0.76 |
| 252 | 242 - 262 | 7.36 | +0.33 | 7.69 | ±0.61 |
| 259.5 | 250 - 269 | 9.35 | +0.28 | 9.63 | ±0.67 |
| 276 | 265 - 287 | 16.12 | +0.19 | 16.31 | ±0.49 |
| 293.5 | 283 - 304 | 19.94 | +0.06 | 22.00 | ±0.94 |
| 300 | 290 - 310 | 26.36 | +0.04 | 26.40 | ±1.6 |

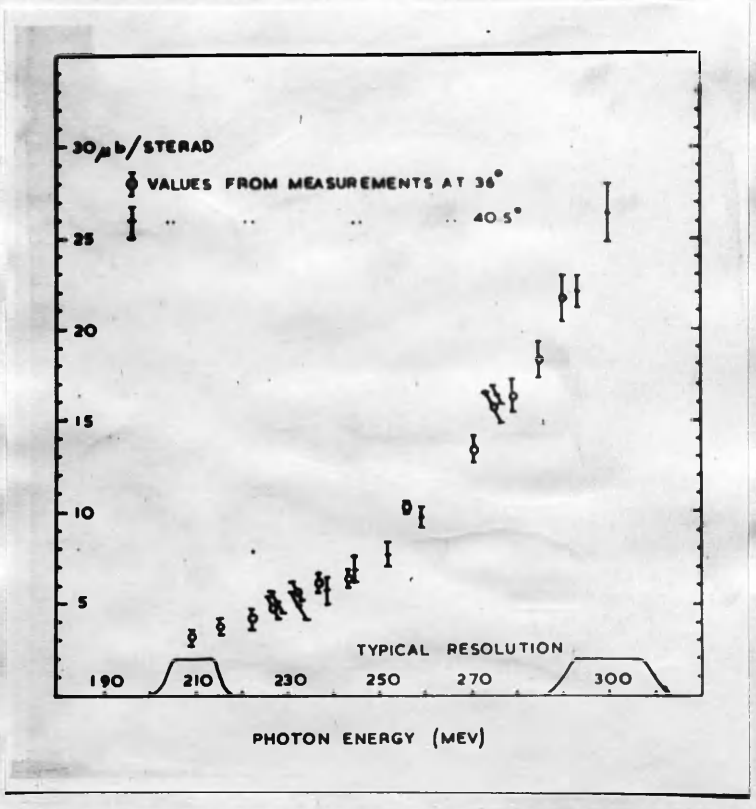
30 μb/STERAD
VALUES FROM MEASUREMENTS AT 36°
" " " " 40.5°
25
20
15
10
5
TYPICAL RESOLUTION
190
210
230
250
270
300
PHOTON ENERGY (MEV)

fig. 23

## Chapter VII

## Discussion and Interpretation of results.

In figure 24 are shown the results of this work together with the relevant portion of figure 1. The horizontal lines about the points indicate the range of photon energy over which A is averaged, the vertical lines the uncertainty in the average A. The results J and Y are taken from a graph in a paper by John and Stoppini (1957) describing an experimental technique and giving these preliminary results. The final results of this have not been published and it is not known what reliance can be put on these. Some results ofYamagata(Y) are also given in this paper. The results S' are taken from a graph in the paper by Smythe et al.(1957). These results were not tabulated in the paper, but nothing indicates that they are any less reliable than the results S of figure 1.

It is seen that the results extrapolate smoothly to those of Vassilkov et al below 200 Mev but not those of Luckey et al.(see figure 25) and at 300 Mev agree with previous measurements. But in the region between, the present results lie lower, being only 70 - 75 % of previously accepted values at 260 - 270 Mev.

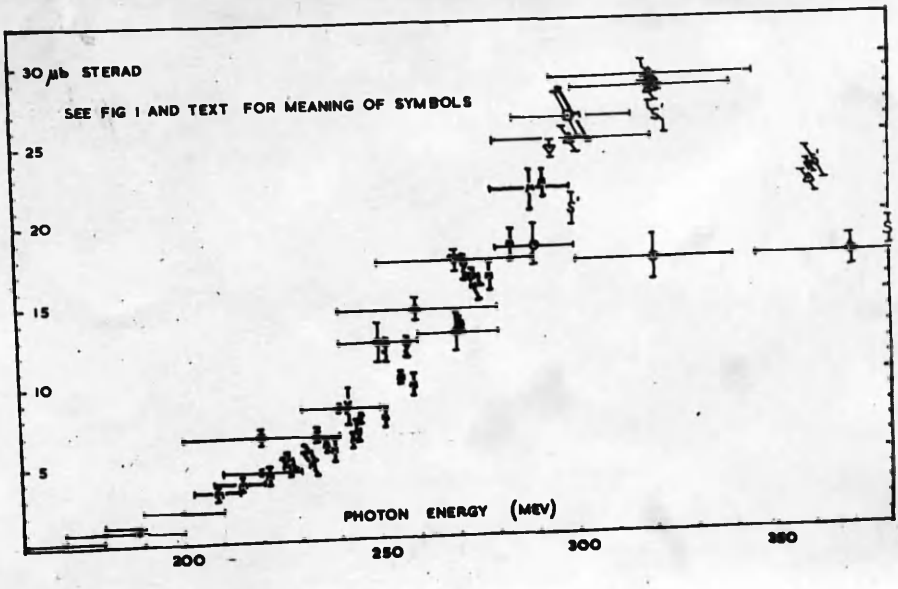
30 μb STERAD
SEE FIG 1 AND TEXT FOR MEANING OF SYMBOLS
25
20
15
10
5
PHOTON ENERGY (MEV)
200
250
300
350

fig. 24

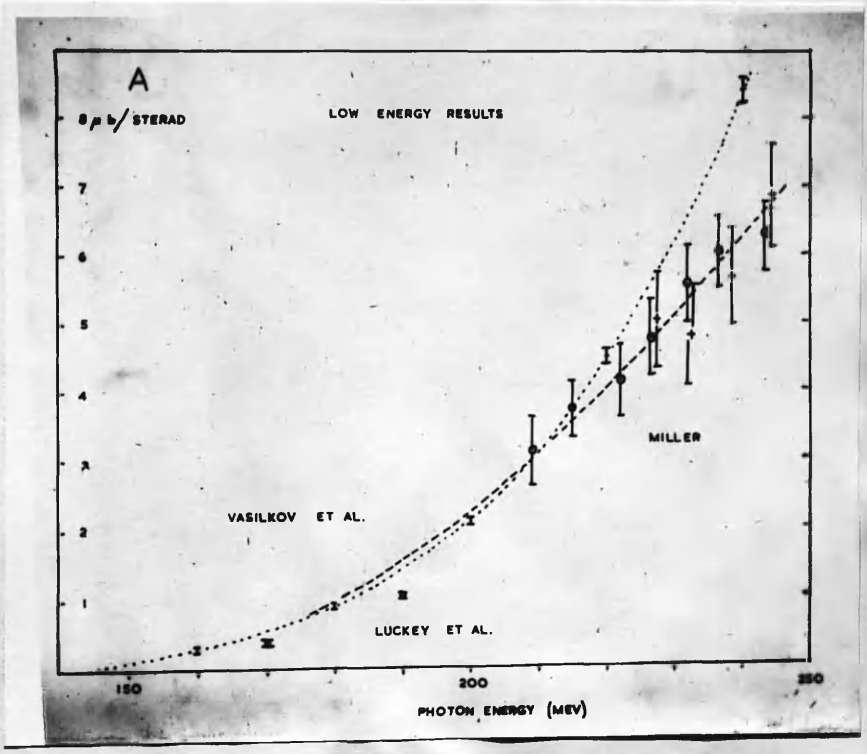
A
8 μ b/ STERAD
LOW ENERGY RESULTS
7
6
5
4
3
2
1
MILLER
VASILKOV ET AL.
LUCKEY ET AL.
150
200
250
PHOTON ENERGY (MEV)

fig. 25

The results of this experiment consist of two almost independent sets. These were made at two different laboratory angles to the target, each with its own background runs, and were analysed separately. At each angle measurements were made by two techniques (measurement of time of flight and energy below 40 Mev, and dE/dx and E above 40 Mev proton energy). At both angles the results of each method run smoothly together without breaks or steps, and when appropriate corrections are made to $90^{\circ}$ in the centre of mass system, the results from the two angles show no significant differences. When the measurements at different angles are thus compared, the values of A obtained originate from protons of different energies, perhaps even different detecting techniques (e.g. the lowest points at both $36^{\circ}$ and $40.5^{\circ}$ to the beam both come from protons $\sim$ 22 Mev energy, but they correspond to photon energies $\sim$ 210 and 230 Mev. figure 23). The good agreement between these makes it unlikely that the apparent discrepancy between these and previous measurements is due to a fault in the counter system or independent parts of the analysis.

The only assumptions in the analysis common to measurements at both angles is the photon spectrum.

As explained in chapter III this was assumed, as a best fit to experimental measurements, to be the Schiff spectrum integrated over all angles, with a slight modification at the high energy end. If this modification is not made, the value of A at the highest energy point is lowered by $\sim$ 8%, the second and third highest by $\sim$ 4% and the effect on the others is negligible . This does not greatly affect the discrepancy.

An error in the absolute calibration of the photon beam intensity will raise or lower all the results by about the same factor. No simple factor like this will improve the agreement. A discrepancy does exist between the two methods available at Glasgow for measuring the absolute beam energy flux. When the ratio of the charge delivered by the Cornell thickwalled ionisation chamber to that delivered by a Quantameter is measured for the same beam flux, this is found to vary from the expected value in an unexplained way by 5% to 15%, depending on the conditions of measurement. The evidence seems to show that the Quantameter is at fault, and that the Cornell chamber is consistent and reliable. Further investigations of this are in progress. All the results in this thesis have been based on the Cornell chamber calibration.

A tentative explanation for the discrepancy between these and previous results is that the photon beam used was partially polarised, with the polarisation varying with photon energy. However in experiments specially set up to detect this effect (Taylor and Mozley (1960)) a maximum effect of 10% in meson yields was found. It is unlikely that with the target and collimator conditions here that this is relevant. A more likely possibility is the Überall effect ( Überall (1956), Frisch and Olson (1959)). If the part of the tungsten synchrotron target used consisted of fairly large crystals ( $\sim$ 1 m.m.), with the correct orientation, then this could give an enhancement of the low energy photon spectrum and a depletion in the 200 - 280 Mev region. This could amount to 10 - 15% for a thin, cooled monocrystalline target, but is unlikely to be more than a few per cent under the conditions of the runs.

The conversion factor for solid angle, from the laboratory system to the centre of mass system, was taken from tables (Malamberg and Koester (1953)) where the $\pi^o$ mass was taken as 136.0 Mev. The changes made by using the modern value of 135.2 Mev are negligible as can be seen by noting that the corresponding solid angle factors for $\pi^o$ and $\pi^+$

mesons at 90° c.m. and 260 Mev are 0.7% different for

$\sim$ 4% difference in mass.

No reasonable alterations in values of solid angle, target thickness, angles of observations, monitor calibration, solid angle factor, counter calibration etc., will produce agreement between the present results and previous ones.

The results of Goldschmidt-Clermont et al., the earliest quantitave results in the field, disagree strongly with all other measurements and will not be further considered here.

As has been pointed out in Chapter II, the previous measurements are not all independent. The values of A have been obtained by fitting an angular distribution function to measurements at angles other than 90° in c.m. Figure 26 shows an experimental angular distribution at $\sim$ 270 Mev. The limits of errors shown include errors of monitoring etc. The point marked "Bernardini" was made during measurements of the proton Compton effect (Bernardini et al.(1960)). The point"M" is taken from the present experiment. It is seen that the discrepancy remains.

Possibilities of error occur in the other measurements. Thus Bernardini's was made with the extreme end of the photon spectrum and so is sensitive to its exact shape. Oakley and Walker had trouble in measuring their low energy

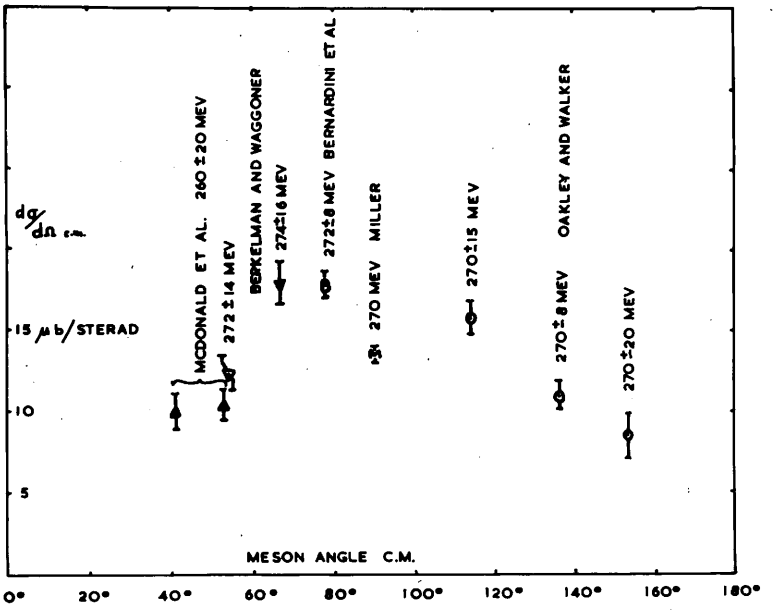
dσ/dΩ c.m.
15 μb/STERAD
10
5
MESON ANGLE C.M.
0°
20°
40°
60°
80°
100°
120°
140°
160°
180°
MCDONALD ET AL. 260 ± 20 MEV
272 ± 14 MEV
BERKELMAN AND WAGGONER
274±16 MEV
272±8 MEV BERNARDINI ET AL
270 MEV MILLER
270±15 MEV
270±8 MEV OAKLEY AND WALKER
270±20 MEV

fig. 26

protons in their experiment because of background and scattering from their lead shielding. The results of Berkelman and Waggoner are normalised to those of McDonald et al.

The results described in this thesis are the only ones made over the complete range of energies from 200 - 300 Mev. They extend the most accurate means of measuring the differential cross-section (proton recoil counting) down to photon energies some 50 Mev lower than previously published reliable results ( discounting Goldschmidt-Clermont et al.).

No systematic error has been found in the performance of the experiment or analysis of the results, and they constitute a self-consistent group, averaged over smaller ranges of photon energies and with better statistical accuracy than most previous results. Further investigations, to be extended to angles other than $90^{\circ}$ c.m. are in progress in this laboratory. This will provide a check on the present results and extend the measurements of C to lower energies by this method.

Accepting the accuracy of the present results has the effect of making the peak in A at about 320 Mev. narrower. The results of De Wire et al. from 300 Mev upwards also tend

to make the peak higher and narrower - see figure 27. In figure 27 the dotted line is a best fit by eye to our results, and the dashed line is the "resonance part" of A, depending on the $\alpha_{33}$ phase shift from scattering data with $f^2 = 0.080$ as calculated by Höhler and Müllensiefen (1959). The two are in good agreement, except near the peak, which means that the contribution of the s-wave and other p-phases must be small, or cancel, or else a different value of $f^2$ must be chosen. Further complications occur when possible pion-pion interactions are taken into consideration, but before this can be clearly demonstrated, the uncertainties in the experimental data must be cleared up.

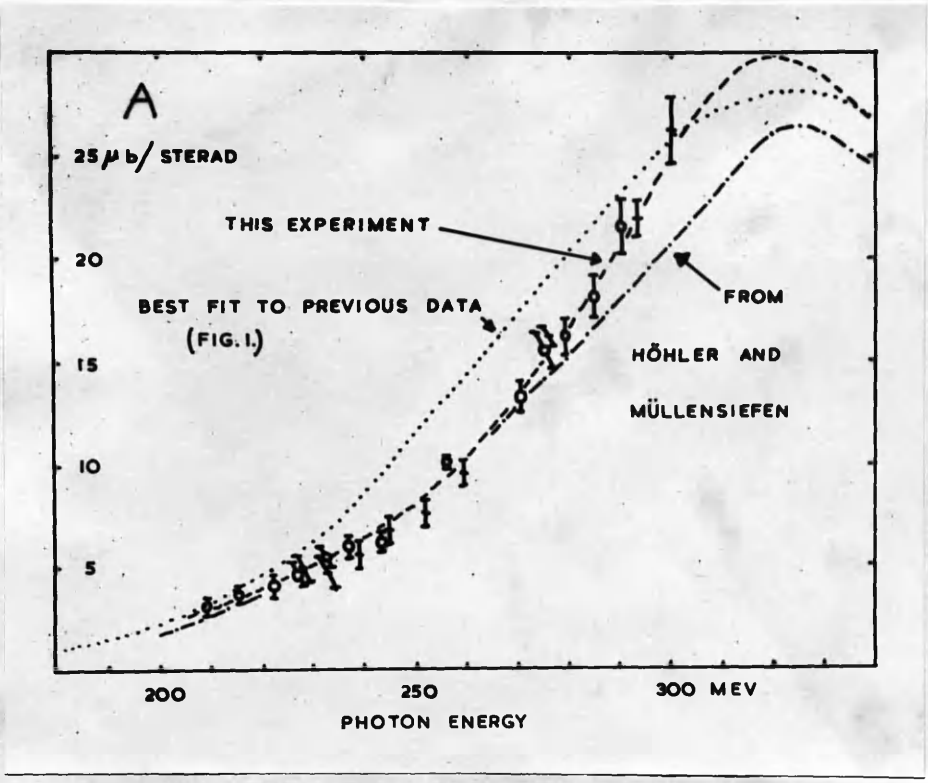
A
25 μb/ STERAD
20
15
10
5
THIS EXPERIMENT
BEST FIT TO PREVIOUS DATA
(FIG. 1.)
FROM
HÖHLER AND
MÜLLENSIEFEN
200
250
300 MEV
PHOTON ENERGY

fig. 27

## References.

Abbreviations.

P.R. = Physical Review.

P.R.L.= Physical Review Letters.

R.S.I.= Review of Scientific Instruments.

N.I.M.= Nuclear Instruments and Methods.

N.C. = Il Nuovo Cimento.

Atkinson, J.R., MacFarlane, W., Reid, J.M. and Swinbank, P. 1957 N.I.M. 1, 152.

Azuma, R.E. and Lewis, G.M. 1957 Philosophical Magazine Vol.8, 2, 1325.

Bellamy, E.H., Hogg, W.R. and Miller,D . 1960 N.I.M. 7, 293.

Berkelman K. and Waggoner J.A. 1960. P.R. 117, 1364.

Bernardini, G. Hanson, A.O., Odian, A.C., Yamagata, T., and Auerbach, L.B. 1960 N.C. 18,1203.

Bernstein, D. and Panofsky, W.K.H. 1956 P.R. 102, 522.

Bethe, H.A. and de Hoffman, F. 1955 "Mesons and Fields II", Row Peterson & Co. N.Y.

Bethe, H.A. and Maximon L.C. 1954
P.R. 93, 768.

Bethe , H.A. and Heitler, W. 1934
Proceedings of the Royal Society A, 146, 83.

Brini, D., Peli, L., Rimondi, O., and Veronesi P.
1955 N.C. 2, supplement, 1048.

Chew, G.F. and Low, F.E., 1956
P.R. 101, 1579.

Chew, G.F., Goldberger, M.L., Low, F.E. and Nambu,Y.
1957. P.R. 106, 1345.

Clement, J.R. and Quinnel, E.H. 1952.
R.S.I. 23, 213.

Cook, L. 1951 R.S.I. 22, 1006.

Cocconi, G. and Silverman, A. 1952.
P.R. 88 , 1230.

Corson, D.R., De Wire, J.W., McDaniel, B.D.,
and Wilson, R.R. 1953.
"The Cornell 300 Mev synchrotron" Cornell

Curtis, C.D. 1953 P.R. 89, 123.

De Wire, J.W. 1959.
"Calibration Data for the Quantameter and the Cornell Thick Walled Ionisation Chamber",Cornell.

De Wire, J.W. and Beach, L.A. 1951.
P.R. 83, 476.

De Wire, J.W., Jackson, H.E., and Littauer, R. 1958.
P.R. 110, 1208.

De Wire, J.W., Feldman, M., Highland, V.L. and Littauer R. 1961. P.R. 124, 909.

Diambrini, G., Figuera, A.S., Rispoli, B., and Serra,A. 1961. N.C. 19, 250.

Dietz, K., Höhler, G. and Müllensiefen ,A. 1960.
Zeitschrift für Physik 159, 77.

Dixon, D.R., and Bandtel, K.C. 1956.
P.R. 104, 1730.

Evans, H.C., and Bellamy, E.H. 1959
Proceedings of the Physical Society 74, 483.

Feld, B.T. 1953 P.R. 89, 330.

Fermi, E. 1950 "Nuclear Physics" p.34
University of Chicago Press.

Fisher, P.C. 1953 P.R. 92, 420.

Frisch, O.R. and Olson, D.N. 1959.
P.R.L. 3, 141.

Goldschmidt-Clermont, Y., Osborne, L.S. and Scott ,M.
1955 P.R. 97, 188.

Gooding, T.J. and Pugh, H.G. 1960.
N.I.M. 7, 189.

Hagerman, D.C. and Crowe, K.M. 1955
P.R. 100, 869.

Hisdal, E. 1957 P.R. 105, 1821.

Hogg, W.R. 1958 Thesis, University of Glasgow.

Höhler G. and Müllensiefen, A. 1959.
Zeitschrift für Physik 157, 30.

John, W., and Stoppini, G. 1957
N.C. 6, 1207.

Koester, L. and Mills, F. 1957
P.R. 105, 1900.

Loeffler, F.J., Palfrey, T.R. and Tantfest, G.W.,
1959 N.I.M. 5, 50.

Littauer, R. 1958 R.S.I. 27, 178.

Luckey, P.D., Osborne, L.S. and Russel, J.J. 1959.
P.R.L. 3, 240.

MacFarlane, W., Barden, S.E. and Oldroyd D.L. 1955
Nature 176, 166.

Malmberg J.G. and Koester, L.J. 1953.
"Tables of nuclear reaction kinematics at relativistic energies", University of Illinois.

McDonald, W.S., Peterson, V.Z., and Corson, D.R. 1957.
P.R. 107, 577.

Miller, D. and Evans , H.C. 1961.
Journal of Scientific Instruments 38, 162.

Nicolai, V.O. 1955 R.S.I. 26, 1203.

Oakley, D.C. and Walker, R.L. 1955.
P.R. 97, 1283.

Olsen, H.,Maximon, L.C. and Wergeland, H. 1957.
P.R. 106, 27.

Panofsky, W.K.H., Aamodt, R.L. and Hadley, J. 1951
P.R. 81, 565.

Panofsky, W.K.H., Steinberger, J.N. and Steller, J.
1952 P.R. 86, 180.

Penfold, A.S. and Leiss, J.E. 1958.
University of Illinois Report May 1958.

Powell, W.M. Hartsough, W. and Hill, M. 1951.
P.R. 81, 213.

Rich, M. and Madey, R. 1954 UCRL report 2301.

Rutherglen, J.G., Walker, J., Miller , D. and
Paterson, E. 1960 Report of Rochester
Conference 1960.

Schiff, L.T . 1946 P.R. 70, 87.

Schiff, L.I. 1951 P.R. 83, 252.

Silverman, A. and Stearns, M. 1952 P.R. 88, 1225.

Sirlin, A. 1957 P.R. 106, 637.

Smythe, R., Worlock, R.M. and Tollestrup, A.V.
1957 P.R. 109, 518.

Stein, P.C. and Rogers K.C. 1958
P.R. 110, 1209.

Steinberger, J.N., Panofsky , W.K.H. and Steller, J.
1950 P.R. 78, 802.

Taylor R.E. and Mozley, R.F. 1960
P.R. 117, 835.

Überall, H. 1956 P.R. 103, 1055.

Vassilkov, R.G., Govorkov, B.B. and Goldansky V.I.
1959 Journal of Experimental and Theoretical
Physics 37, 11 (10, 7 in translation).

Vette, J.I. 1958 P.R. 111, 622.

Walker, J.K. 1961 Thesis, University of Glasgow.

Walker, R.L., Oakley, D.C. and Tollestrup, A.V.
1955 P.R. 97, 1279.

Wexler, A. and Corak, W.S. 1951 R.S.I. 22, 941.

Whalin, E.A.and Reitz, R.A. 1955 R.S.I. 26, 59.

Whalin, E.A., Schriever, B.D. and Hanson, A.O.
1956 P.R. 101, 377.

Wheeler, J. and Lamb, W. 1939 P.R. 55, 858.

White, R.S., Jacobson, M.J. and Schulz, A.G. 1952
P.R. 88, 836.

Wilson R.R. 1957 N.I.M. 1, 101.

Wooley, H.W., Scott, R.B. and Brickwedde, F.G. 1948
Journal of Research of the National Bureau of

Standards 41, 379.